

# **COLLISION RISK PREDICTION UTILIZING ROAD SAFETY MIRRORS AT BLIND INTERSECTIONS**

**Noriaki, Itagaki**

Continental Automotive Corporation  
Japan

**Shintaro, Ono**

The University of Tokyo / Fukuoka University

**Yoshihiro, Suda**

The University of Tokyo  
Japan

**Kazuya, Okawa**

Chiba university  
Japan

**Ralph Grewe**

Continental AG  
Germany

Paper Number 23-0164

## **ABSTRACT**

Traffic accident number in Japan has been reduced year by year by growing ADAS technologies, revising the traffic rules, improving traffic environment. However, to realize the Vision Zero world which is zero traffic accidents, zero fatal accidents and zero injured seems far away currently. According to the traffic accident statistics data in Japan, more than half of accidents are occurring both in and around intersection areas [1]. The accident number at the intersections without traffic light is bigger than that with traffic light and has been seen at residential areas. To reduce the accident number at the intersection without traffic light, road safety mirrors have been installed in the intersection frequently [2]. In our study, using the front camera, which is one of ADAS sensors, even if it is a scene where the front camera cannot detect the object directly, our purpose is to reduce the collision risk by detecting the approaching vehicle using its image in road safety mirrors.

In this paper, our collision avoidance method which consists of the 3 steps "Road safety mirror detection", "Object detection in the road safety mirror" and "Risk prediction" has been proposed. Especially, in road safety mirror detection, one countermeasure for false positives (FP) has been introduced. Our proposed method has

been verified using front camera as a feasibility study, and the effectiveness of our proposed method has been demonstrated by experimental results on the public road. If the effectiveness of our proposed method is proven, since road safety mirrors will be utilized, which are a legacy infrastructure element, new investment at poor visibility intersection can be reduced which will be one of the merits of the proposed method. Also, the scalability of the system supporting not only Autonomous Driving (AD) systems of level 3 and higher, but also AD level 1 and 2 such as Advanced Driver-Assistance System (ADAS) will be an advantage.

### 1. SYSTEM OPERATIONAL CONCEPT FOR T-CROSSING WITH ROAD SAFETY MIRROR

Road safety mirrors can be frequently seen at poor visibility intersections in Japan. In other words, road safety mirrors can be seen at intersections which seem to have a high collision risk. This paper is focusing on collision avoidance at road safety mirror equipped intersections which is one of Japan specific environments. And, we have been focusing on the analysis of reflected images of road objects in the road safety mirror. For collision avoidance by using the reflection in the road safety mirror, our proposed method has been expected to support the recognition of road objects out of the direct field-of-view from the front camera at poor visibility intersection.

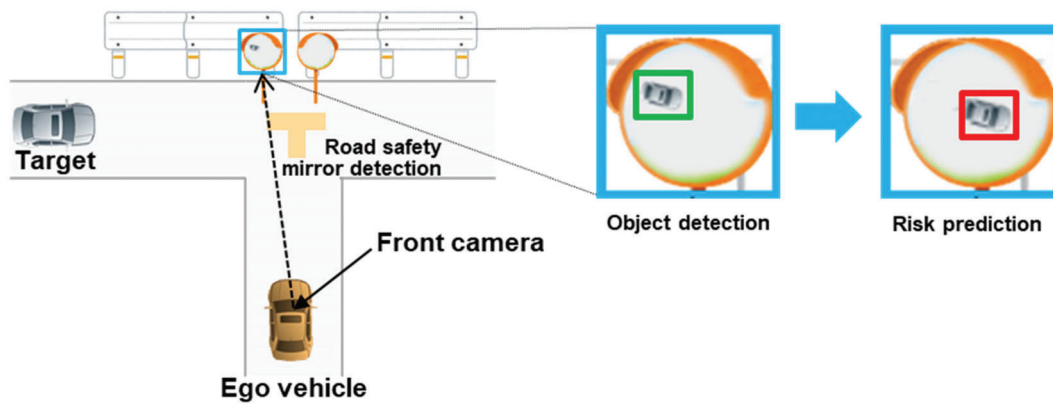


Figure 1. System purpose.

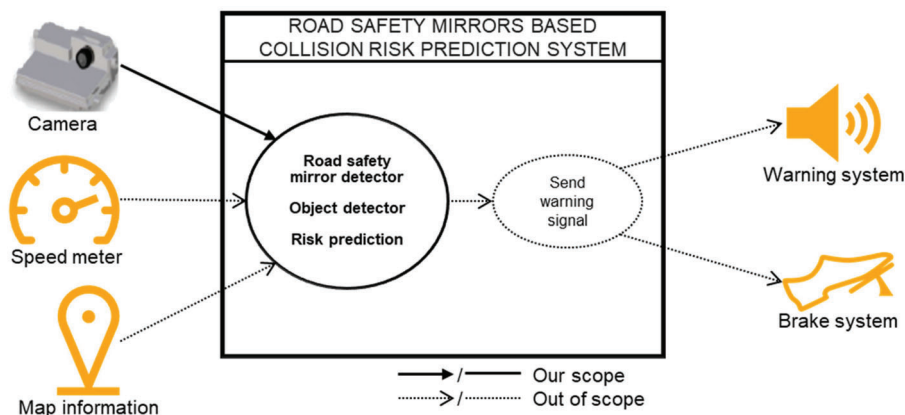


Figure 2. System scope from use-case and actor perspectives.

### 1.1. System Purpose

The purpose of this system is, for example, to support detection of approaching vehicles, to estimate the risk of collision, and to give the risk information to the driver through a driver warning system. Figure 1 shows the system context which shows a situation for the mitigation of predicted risk using the road safety mirror at a T-crossing. The front camera of the ego vehicle detects the road safety mirror and extracts the piece of the image containing the reflected approaching target vehicle on the road safety mirror. When the target vehicle is approaching, it is estimated that there is a high collision risk, which is the case shown by the red square in right side picture in Figure 1.

### 1.2. System Context

Figure 2 shows the system scope and interaction between scope of interest and external systems. Our study scope in this paper is the software algorithm including the road safety mirror detector, the object detector within detected road safety mirrors and the risk prediction at the T-crossing if the target object is a passenger vehicle. It means it does not include the interface to the vehicle speed meter, brake system, map information or to a warning system for sending a signal. The calculation of the estimated collision risk is based on image data from the front camera. The system is enabled based on a trigger by a defined threshold of the ego vehicle speed. When it detects a high collision risk target vehicle is approaching, the system sends a warning signal to inform the driver. Additionally, the system can have an interface to the brake system because it can be utilized to give brake assistance for the driver. For the system it is also desirable to have a map information interface because the map is expected reduce FP and false negative (FN) events.

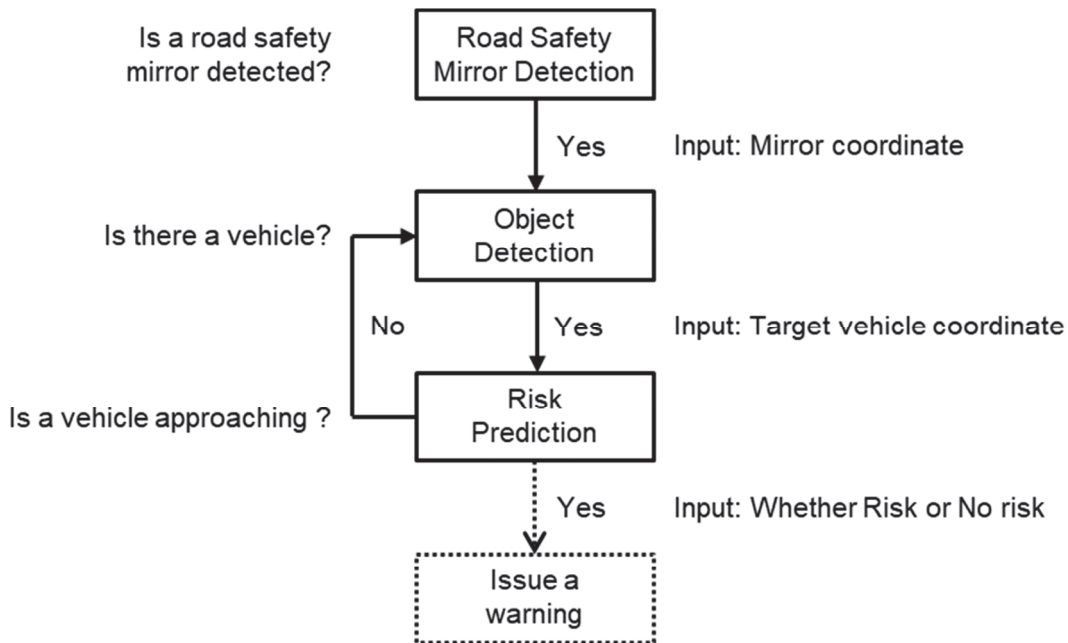


Figure 3. Schematic flow of our system.

## 2. PROPOSED SYSTEM FUNCTION

Figure 3 shows a schematic flow of our system. When the system detects a road safety mirror, it starts to search for a vehicle on the road safety mirror. At this time, if it detects a target vehicle reflected in the road safety mirror, it is transitioning to risk prediction. Risk prediction is an algorithm that determines whether the target vehicle in the road safety mirror is approaching and, if it determines that it is approaching, issues a warning to the driver. For the road safety mirror detection, not only a detection approach using YOLOv3 [3] but also FP prevention by applying Deep Autoencoding Gaussian Mixture Model (DAGMM) [4] has been developed. For road object detection in the road safety mirror, Faster-RCNN (F-RCNN) [5] has been selected, and a risk prediction method which applies interpolation by a Kalman filter and object tracking [6] is applied in this paper. Additionally, although it has been not applied in this paper, an enhanced approach for risk prediction [7] has also already been published.

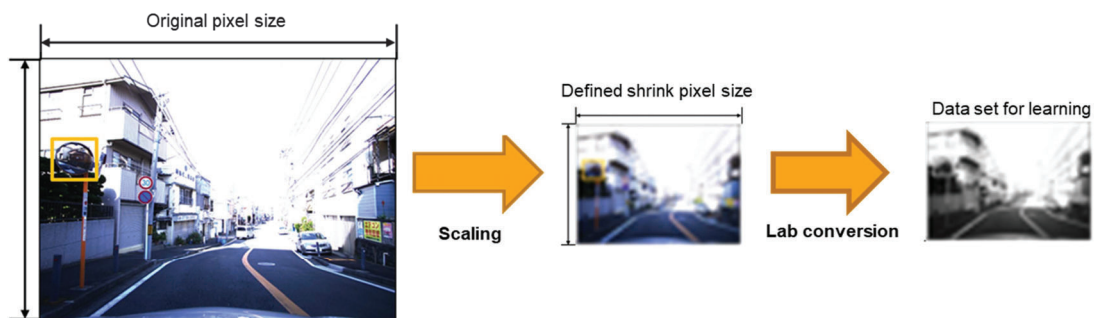


Figure 4. Data set preparation for road safety mirror detection using YOLOv3.





Figure 5. One frame shot of verification result of road safety mirror detection.

### 2.1 Road Safety Mirror Detection

For road safety mirror detection, YOLOv3, which is one of the well-known deep learning methods, in its latest version as of 2019 has been selected. For learning data, it has been using high resolution pixel image (approximately 12 M pixel) and the Region of Interest (ROI) information of the road safety mirror has been

included. The ROI means the area where we are searching a potential target object is a box around the detected road safety mirror like enclosed in the yellow square in Figure 4. The original image will be scaled to a defined reduced size and converted to L\*a\*b\* [8] color space image as shown in the left side picture in Figure 4. Here, RGB means color based on red, green, blue colors. Capital L\* of L\*a\*b\* means luminosity and small a\*, b\* means complementary colors. The L\*a\*b\* color space seems to be closer to human visual. In RGB, it is sometimes hard to distinguish colored areas depending on the brightness situation. On the other hand, in L\*a\*b\* it might be possible to distinguish the color areas like in human vision. Thus, in this paper, the L\*a\*b\* color space is the input for the deep learning method which has been applied.

**Table 1.**  
**Verification result of road safety mirror detection**

True positive (TP)	False positive (FP)
e.g., 	e.g., 
696 detections	35 detections

**2.1.1. Public-road-running-test** Public road tests have been executed using a low-resolution camera (approximately 0.32 M pixel) which is different from the high-resolution camera used for data collection. As controller, a NVIDIA Jetson Xavier has been used. Nevertheless, the results seem to have very good precision of more than 95% as described in Table 1 and Equation (1). Figure 5 shows the one frame shot of verification results of road safety mirror detection.

$$Precision = \frac{TP}{TP+FP} = \frac{696}{696+35} = 95.2\% \quad \text{Equation (1)}$$

Although it is not so many issues, we can see some FP in these results. In the next section, the countermeasure to reduce the FP issues is described.

**2.1.2. Countermeasure-to-false-positive** The countermeasures to FP issues are described in this section. A FP is one of the issues which often limits performance in this perception field. In order to reduce the FP issues, an anomaly detection method has been used. Recently, the Deep Autoencoder Gaussian Mixture Model (DAGMM) has been published (2018). By using a Gaussian Mixture Model, we can find a cluster of features for each object.

However, the mirror image is inconsistent. So, it was hard to define the distribution of the road safety mirrors features in comparison with traffic sign features. Thus, in order to overcome this issue, we have created the opposite idea to a conventional approach. Figure 6 is just an example to explain our approach. If the red points in Figure 6 are assumed to be clusters of traffic signs features, the black points close to these clusters might also

be a traffic sign. Our proposed method estimates that the points far away from these clusters might be road safety mirrors. After detecting potential road safety mirrors by the deep learning method YOLOv3, we calculate their distance to these red clusters. If the distance is over the defined threshold, the system regards the detected object is road safety mirror. If the distance is within the defined threshold, the system regards the detected object is not a road safety mirror.

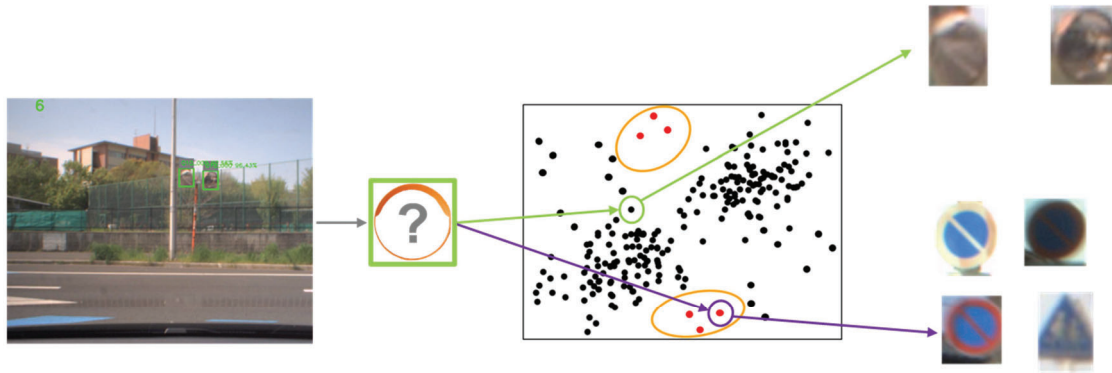


Figure 6. Our proposed approach for detecting the road safety mirror to reduce the false positive



Figure 7. Effectiveness of our proposed approach applying DAGMM



Figure 8. Road safety mirror detection by our proposed approach applying DAGMM

Figure 7 (a) shows the result for a part of a recording without DAGMM. As the result, FP count was 31 in this recording. On the other hand, the right picture in Figure 7 (b) shows the result for the part of the recording with DAGMM as proposed by our approach. FP was zero counts based on the same recording. The effectiveness by our proposed method was proved by this recording. Furthermore, the road safety mirror detection by our proposed method applying DAGMM has been confirmed after approaching to the T-crossing as shown in Figure 8. As summary in road safety mirror detection, it has been verified that the FP count can be effectively reduced, and road safety mirrors can be detected by using our proposed method.

## 2.2. Road object Detection in Road Safety Mirror

In order to detect road objects, the deep neural network Faster R-CNN has been used. For the feature extraction in Faster R-CNN, Resnet 50 is used here. It is a deep residual network to handle the problem of vanishing/exploding gradients[9][10][11]. The basic unit is shown in Figure 9, which has better performance in small objects detection [12].

In this paper, we use a pre-trained Faster R-CNN with Resnet 50 model [13] based on the Microsoft Coco dataset [14]. The following 7 classes are targeted for road objects, which are the most-seen objects on roads in Japan:

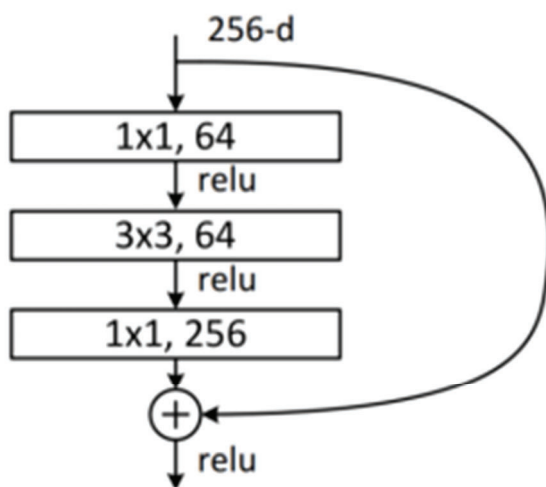


Figure 9. Basic unit of Resnet 50

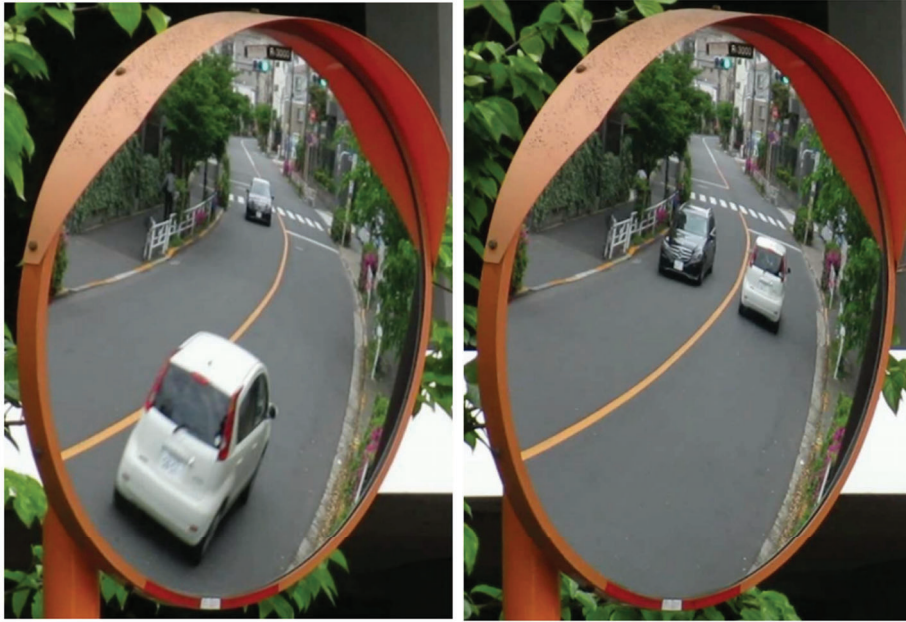


Figure 10. Moving objects in road safety mirror

Table 2.

Relationship between local direction and risk level

Local direction of objects	Risk level of objects
Up to down	High
Down to up	Low

- (1) Pedestrian (person)
- (2) Bicycle
- (3) Car
- (4) Motorcycle
- (5) Bus
- (6) Train
- (7) Truck

### 2.3. Risk Prediction

For human drivers, the road safety mirror is a tool to confirm if there is any object like vehicle or pedestrian coming with a possible collision risk. The direction of a moving object in the road safety mirror is a critical factor to decide whether it has potential collision risk for the driver. As shown in Figure 10, while the black vehicle moves from top to bottom in vertical direction in the road safety mirror, it is coming closer to the road safety mirror, which has relatively high collision risk for the ego vehicle. On the contrary, while the white



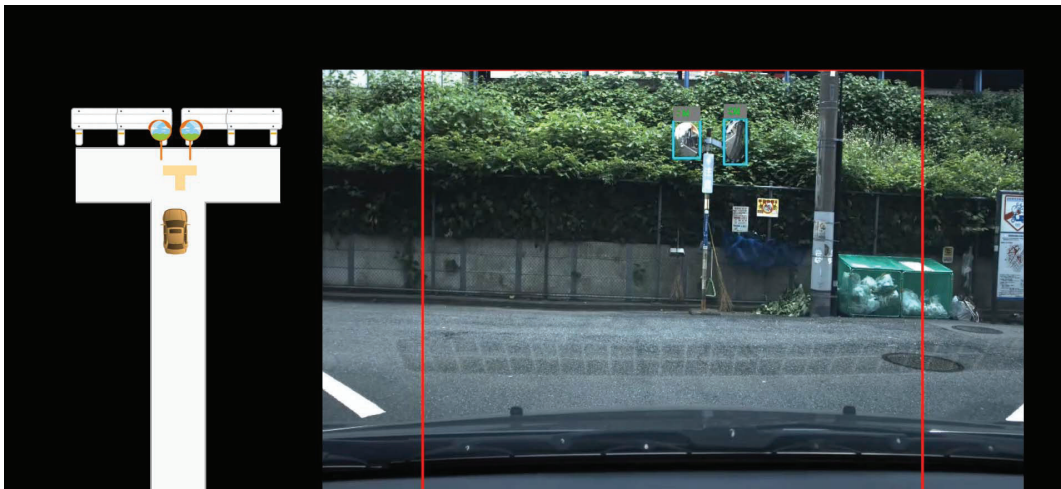
vehicle moves from bottom to top in vertical direction in the road safety mirror, it is going away from the road safety mirror, and the risk to collide with the ego vehicle is relatively low. As a result, by detecting the moving direction of an object in the road safety mirror (called local direction), it can be estimated whether the object is coming near or heading away, which can be used for the classification as a high-risk object or a low-risk object, respectively. The local direction of an object has been calculated from the track of the object obtained in described in Reference [6]. The correspondence relationship between local direction and risk level of objects is described in Table 2.

### 3. EXPERIMENTAL RESULTS

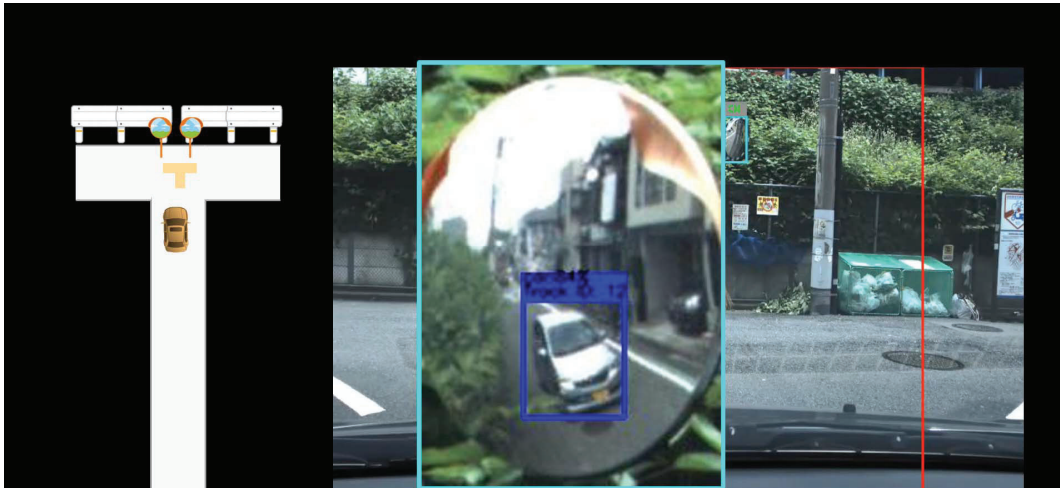
To verify the effectiveness of our proposed method, public road tests have been executed using a high-resolution camera (approximately 20 M pixel). Although the resolution might be reduced, this high-resolution camera has been selected to verify the feasibility of our proposed method which is object detection in the road safety mirror and the risk prediction in first combined tests on the public road.

Figure 11 shows the experimental result of the road safety mirror detection. Figure 12 shows the experimental result of the object detection in the road safety mirror. Figure 13 shows the experimental result of risk prediction of the target vehicle approaching. It seems that the road safety mirror detection by our proposed method can detect the road safety mirror stably as shown in Figure 11. Also, it seems that the object detection in the road safety mirror by Faster R-CNN which we applied can detect road objects stably as shown in Figure 12. Furthermore, we can see that the risk prediction works as planned as shown in Figure 13.

From the above experimental results for our combined proposed method, our proposed concept for detecting high collision risk of approaching vehicles at T-crossings equipped with a road safety mirror by using only the front camera image have been proven in public road test.



*Figure11. Experimental result of road safety mirror detection*



*Figure12. Experimental result of object detection in the road safety mirror*

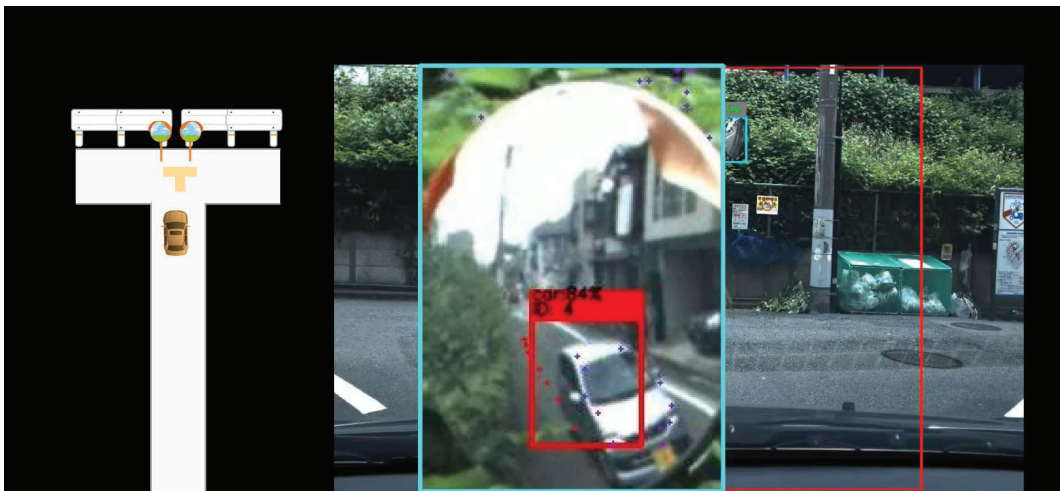


*Figure13. Experimental result of risk prediction to the target vehicle approaching*

#### 4. CONCLUSIONS

In this paper, we propose a method to reduce the collision risk at crossings by detecting approaching vehicles using their reflection in road safety mirrors, using a 3-Step approach consisting of "Road safety mirror detection", "Object detection in the road safety mirror" and "Risk prediction". Our proposed method has been verified using real world camera data as a feasibility study, and the effectiveness of our proposed method has been demonstrated by experimental results at T-crossing on public roads. Considering these results, it will be expected that our proposed method improves safety while avoiding new investments at poor visibility intersections and can be adapted to any levels of AD/ADAS system. The next steps considered are to improve robustness in different weather and illuminance conditions, to add more classes of target objects and to bring maturity closer to production level.

## REFERENCES

- [1] Institute for Traffic Accident Research and Data Analysis, J-TAD, 2017. [online], Available: ["http://www.itarda.or.jp/materials/publications.php?page=4"](http://www.itarda.or.jp/materials/publications.php?page=4)
- [2] Douro Hanshyakyo Kyokai (Japan Traffic Convex Mirror Association) [online], Available: ["https://www.dhk.gr.jp/"](https://www.dhk.gr.jp/)
- [3] YOLO (You Only Look Once) [online], Available: ["https://pjreddie.com/darknet/yolo/"](https://pjreddie.com/darknet/yolo/)
- [4] Zong, B., Song, Q., Min, M. R., Cheng, W., Lumezanu, C., Cho, D. and Chen, H. 2018. "Deep Autoencoding Gaussian Mixture Model for Unsupervised Anomaly Detection." 6th International Conference on Learning Representations (Vancouver Convention Center, Vancouver, BC, Canada April 30 - May 3). Poster Papers
- [5] He, K. et al. 2015. "Deep residual learning for image recognition." Proceedings of the IEEE conference on computer vision and pattern recognition, pp.770-778
- [6] Ono, S., Feng, Y., Suda, Y. and Itagaki, N. 2020. "Detection of Risky Events at Blind Spots on Roads using On-vehicle Camera and Road Safety Mirror." 2020 JSAE Annual Congress (Spring), 20205065
- [7] Hino, Y., Ono, S., Itagaki, N. and Suda, Y. 2021. "Recognition of Risky Events Reflected in Road Safety Mirror Considering Ego Vehicle's Motion", 7th International Symposium on Future Active Safety Technology toward Zero Accidents (FAST-zero), 20219028
- [8] CIE Colorimetry - Part 4: 1976 L\*a\*b\* Colour Space, 2nd Edition, 2007 [online], Available: ["http://cie.co.at/publications/colorimetry-part-4-cie-1976-lab-colour-space-0"](http://cie.co.at/publications/colorimetry-part-4-cie-1976-lab-colour-space-0)
- [9] Bengio, Y. et al. 1994. "Learning long-term dependencies with gradient descent is difficult." IEEE Transactions on Neural Networks, Vol.5, No.2, pp.157-166
- [10] Glorot, X. and Bengio, Y. 2010. "Understanding the difficulty of training deep feedforward neural networks." Proceedings of the thirteenth international conference on artificial intelligence and statistics, pp. 249-256
- [11] Huang, J. et al. 2017. "Speed/accuracy trade-offs for modern convolutional object detectors." Proceedings of the IEEE conference on computer vision and pattern recognition, pp. 7310-7311
- [12] Pang, J. et al. 2019. "CNN: Fast Tiny Object Detection in Large-Scale Remote Sensing Images." IEEE Transactions on Geoscience and Remote Sensing, arXiv:1902.06042
- [13] Github, Tensorflow detection model zoo [online], Available: ["https://github.com/tensorflow/models/blob/master/research/object\\_detection/g3doc/detection\\_model\\_zoo.md"](https://github.com/tensorflow/models/blob/master/research/object_detection/g3doc/detection_model_zoo.md)
- [14] Lin, T. et al. 2014. "Microsoft coco: Common objects in context, European conference on computer vision." Springer, Cham, pp.740-755

# MOTORCYCLE STATE ESTIMATION USING VISUAL-INERTIAL ODOMETRY

Martin Pryde  
Lamri Nehaoua  
Hicham Hadj-Abdelkader  
Hichem Arioui

Laboratoire IBISC, Université d'Evry Val-d'Essonne, Université Paris-Saclay  
France

Paper number 23-0225

## ABSTRACT

The authors propose a visual-inertial algorithm to estimate the kinematic states of a motorcycle traveling at high speeds along an extra-urban road. The approach comprises the following steps: First, a monocular camera takes video of the road ahead. Key features from sequential video frames of the road surface are extracted using the Harris corner detector. Matching features are identified using the Fast retina keypoint descriptor (FREAK). Next, correct the perspective warping of the feature locations by applying inverse perspective mapping. The motion of the transformed features is registered using the Singular Value Decomposition (SVD) variant of the Iterative Closest Point (ICP) algorithm. Finally, this measurement is combined with readings from inertial navigation system using a Kalman filter to produce a filtered estimate and correct integrator drift. The approach was validated using data from simulations of three scenarios created in BikeSim. In the first, the motorcycle performs a series of slaloms along a straight road at 50 km/h. In the second, the motorcycle navigates an S-shaped bend at 80 km/h. Lastly, the motorcycle performs a double-lane change across both lanes of a straight road at 110 km/h.

## INTRODUCTION

The term *Powered Two-Wheeled Vehicles* (P2WV) encompasses the class of self-propelled road vehicles whose two wheels are arranged in tandem. *Riders* of P2WVs continue to be overrepresented in severe road accidents [1]. By contrast, automobile road safety has steadily improved over the past decade. Among many factors in this trend has been the introduction of Advanced Driver Assistance Systems (ADAS) into modern cars [2]. In this context, researchers at the IBISC laboratory are investigating the modeling and control of P2WVs with the aspiration of developing technologies for *Advanced Rider Assistance System (ARAS)*. Various rider aids are already commercially available such as Forward Collision Warning (FCW) and Adaptive Cruise Control (ACC) that are analogous to their automobile counterparts. We are particularly interested in developing an ARAS analog of the *Electronic Stability Control* (ESC) now ubiquitous among recent car models. Consider a warning system capable of detecting and alerting the rider to dangerous steering situations. In critical situations, such a system could even intervene semi-autonomously to mitigate an accident.

Developing such a system is not as simple as implementing existing ESC on motorcycles: Their slim profiles permit a larger envelope of lateral motion compared to a car. Furthermore, a novice rider often has trouble judging the appropriate lateral position and heading relative to the road to safely navigate a bend. Hence, riders can attain larger magnitudes of relative lateral velocity compared to cars. Consider also that a rider must not only judge their trajectory but must also *lean* into a turn to balance out the overturning moment caused by the road-tire interaction. Therefore, the key difference from cars is that the body lateral velocity, yaw rate and steering angle can no longer be assumed to act in the road plane. Alternative formulations for the front and rear wheel *slip angles*, the angles formed between the direction in which a wheel is pointing and in which it is traveling, must be used for an ESC equivalent for P2WVs to effectively characterize dangerous over and under-steering behaviors.

*Visual-Inertial Odometry* (VIO) has shown encouraging performance in measuring translational velocities in *Uncrewed Aerial Vehicles* (UAVs) [3]. VIO estimates *ego-motion* in real-time using a camera alongside an *Inertial Measurement Unit* (IMU). The readings from these sensors are fed to a motion estimation algorithm such as *Optical Flow* (OF), the *Direct Linear Transform* (DLT) and *Iterative Closest Point* (ICP). Research has also been conducted into implementing VIO for *Uncrewed Ground Vehicles* (UGVs). The planar constraints of UGVs simplify the motion estimation problem to two dimensions compared to UAVs. VIO for UGVs has shown promise during indoor navigation tasks performed across multiple works [4],[5]. Outside of laboratory conditions, the works of Song et al. show a real-world demonstration of VIO for a small UGV capturing video of the ground beneath itself. We note that to date, these implementations were conducted only at low speeds ( $\leq 50$  km/h).

We take inspiration from VIO for UAVs alongside the work conducted thus far for UGVs and investigate its potential in the real-time estimation of velocity for P2WVs. We seek to know if the VIO algorithms which perform well at high velocities on UAVs perform comparably on a motorcycle. Previous works from IBISC have investigated the use of Inverse Perspective Mapping (IPM) to further simplify the motion estimation problem for road vehicles [6]. Thus, we summarize our estimation algorithm: We extract matching features from successive images taken by a camera mounted on the front of a motorcycle. Next, we use IPM to remove the perspective warping from the feature sets and obtain two point sets. We apply ICP to estimate the rigid transform between these two sets. From here, we express this motion estimate in the body frame of the motorcycle and use it as the drift-correcting component of a Kalman filter-based *Inertial Navigation System* (INS). Finally, we re-express this filtered estimate in the road plane and apply the appropriate kinematic expressions for P2WVs to calculate the wheel slip angles.

## Motivation

Referring to the seminal works on motorcycle dynamics by Cossalter et al. [7], we define two cornering radii: The *ideal* radius  $R_0$  of the path taken by the motorcycle assuming there is no lateral wheel slip and the actual path radius  $R$ . The ratio of these is termed the *steering ratio*  $\xi$  and defines whether a motorcycle is over, neutral or under-steering as shown in (1). Cossalter et al. derives and validates the approximations for these radii in kinematic terms shown in (2) and (3) where  $\alpha_f$  and  $\alpha_r$  are the front and rear slip angles respectively [8].

$$\xi = \frac{R_0}{R} \begin{cases} \xi < 1 & \text{under-steering} \\ \xi = 1 & \text{neutral steering} \\ \xi > 1 & \text{over-steering} \end{cases} \quad (1)$$

$$R_0 = \frac{l_{wb}}{\tan \Delta} \quad (2)$$

$$R = \frac{l_{wb}}{\tan(\Delta - \alpha_r) \cos(\alpha_r) + \sin(\alpha_f)} = \frac{V}{\dot{\psi}} \quad (3)$$

The definitions for all symbols used in this work are listed in Table 1.  $V$  is the *velocity magnitude* defined as the norm of the longitudinal and lateral body velocity components (4). Care should be taken to distinguish the handlebar steering angle  $\delta$  from its projection onto the road plane  $\Delta$  termed the *kinematic steering angle* which can be well-approximated using (5).

$$V = \sqrt{v_x^2 + v_y^2} \quad (4)$$

$$\Delta = \arctan\left(\frac{\cos(\epsilon)}{\cos(\varphi)} \tan(\delta)\right) \quad (5)$$

Relationships first derived by Robin Sharp express the front and rear slip angles in terms of the kinematic variables defined thus far. Note that in (6) and (7) as well as in (4) the longitudinal and lateral components  $v_x$  and  $v_y$  are expressed in the road plane and correspond to the velocity of the *projection* of the motorcycle Center of Mass (CoM) onto this plane.

$$\alpha_f = \arctan\left(\frac{v_y + l_f \dot{\psi} - l_{tr} \dot{\delta}}{v_x}\right) - \delta \cos(\epsilon) \quad (6)$$

$$\alpha_r = \arctan\left(\frac{v_y - l_r \dot{\psi}}{v_x}\right) \quad (7)$$

Thus one concludes that accurate measurements of velocity, yaw rate and steering angle are essential when attempting to estimate the slip angles. Steering angle and rate can be obtained using a position encoder in the steering bearing while the yaw rate can be accurately measured by even low-cost MEMS gyroscopes. However, velocity is a more challenging state to reconstruct: One can suppose that longitudinal velocity can be measured by the vehicle's engine odometer under the assumption that there is no longitudinal slip between the tires and the road. Lateral velocity is more challenging still: Many approaches assume the availability of this state through *Global Navigation Satellite System* (GNSS). In reality, the latency and precision of most consumer GNSS modules are, on their own, inadequate for real-time estimation and control applications according to tests carried out by the Connected Motorcycle Consortium (CMC) at the Technische Hochschule Ingolstadt in Germany [9].

**Table 1.**  
*List of states and their definitions (absent of point and frame definitions)*

symbol	state	units	symbol	parameter	units
$\mathbf{a}$	translational acceleration	m/s <sup>2</sup>	$l_f$	arm between $G_r$ and $C_f$	m
$\boldsymbol{\omega}$	angular velocity	rad/s	$l_r$	arm between $G_r$ and $C_r$	m
$\mathbf{v}$	translational velocity	m/s	$l_{rk}$	rake	m
$\phi$	roll	rad	$l_{tr}$	normal trail $R_f \sin(\epsilon) - l_{rk}$	m
$\theta$	pitch	rad	$R_f$	front wheel radius	m
$\psi$	yaw	rad	$R_r$	rear wheel radius	m
$\varphi$	lean	rad	$\epsilon$	caster angle	rad
$\delta$	steer	rad	$\mu$	camera tilt	rad
$\Delta$	kinematic steer	rad	$l_{wb}$	wheelbase $l_f + l_r$	m
$\alpha_f$	front slip	rad			
$\alpha_r$	rear slip	rad			

State observer approaches hypothesize that it is possible to reconstruct lateral velocity from measurements of other states and a sufficiently faithful dynamical model. The most widely used of these is the Sharp 1971 linearized model [10]. However, observers based on the Sharp model and variations of it have delivered mixed results to date across multiple works [11],[12],[13]. Ahead of this work, we re-confirmed the results of [12] in Figure (1) by implementing their *Linear Parameter-Varying* (LPV) variant of the Sharp model and comparing against results from BikeSim. We note that while the yaw and lean dynamics estimates are satisfactory, the estimate for the lateral velocity deviates significantly from the ground truth. Furthermore, model-based observers rely on accurate *a priori* knowledge of P2WV dynamic parameters, such as mass and moment of inertia, which vary widely depending on the rider [14]. Hence, a key technical motivation for this work is to obtain a more accurate and robust result for lateral velocity compared to available model-based observer approaches.

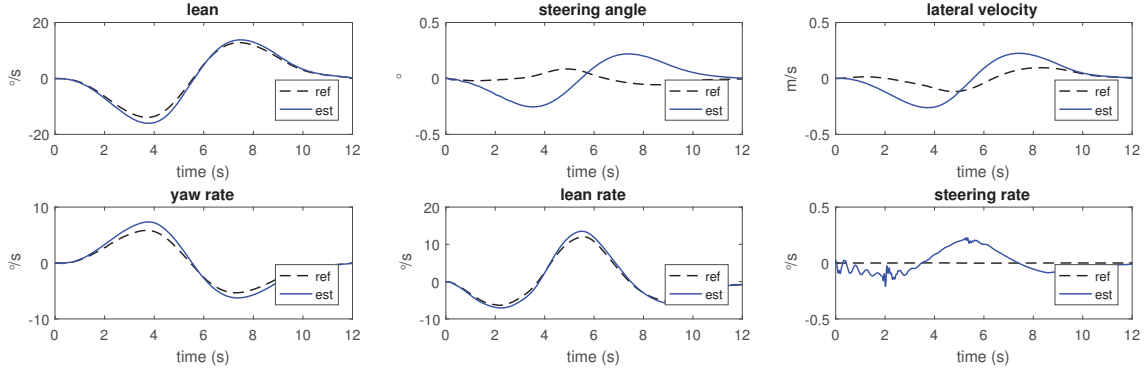


**Figure 1.** Lateral motion results for an LPV model of a motorcycle. Note the significant deviation from ground truth lateral velocity in the top right plot.

## Notation

We summarize the notation used in this work as follows:

- The frame originating from the point  $P$  is denoted  $\mathfrak{R}_P$ .
- $\mathbf{x}$  and  $\boldsymbol{x}$  are column vectors while  $\mathbf{A}$  and  $\boldsymbol{A}$  are matrices.
- The position vector  $\boldsymbol{p}_a^b \in \mathbb{R}^3$  is the Euclidean position of the point  $a$  expressed in  $\mathfrak{R}_b$ .
- The distance vector  $\boldsymbol{r}_{a,b}^b$  begins at point  $a$ , ends at point  $b$  and is expressed in  $\mathfrak{R}_b$ .
- The time derivative of  $\boldsymbol{p}_a^b$  is  $\dot{\boldsymbol{p}}_a^b$ .
- the velocity vector  $\boldsymbol{v}_a^b$  is the velocity of the point  $a$  expressed in  $\mathfrak{R}_b$ .
- $\mathbf{A}^T$  is the transpose of  $\mathbf{A}$  while  $\mathbf{A}^{-1}$  is it's inverse.
- We favor the skew-symmetric operator  $[\mathbf{x}]_{\times}$  over the cross product  $\times$ .
- The identity and null matrices are denoted by  $\mathbf{I}$  and  $\mathbf{0}$  respectively.
- The det operator returns the determinant of a matrix.

## SYSTEM DESCRIPTION

Consider a motorcycle traveling at high speed along an extra-urban road. We propose to attach a monocular camera in front of the steering head fixed to the motorcycle rear body as shown in Figure 2. When the *lean*  $\varphi$  of the motorcycle is zero, the camera is located at a height  $h_0$  above the road and at a distance  $l_f$  from  $G_r$  shown in Figure 3. Concerning environmental conditions, assume the road surface is smooth and well-illuminated in good weather so that no raindrops and little jitter are present in the camera images.

Additionally, we consider that this motorcycle is fitted with an IMU located at the Center of Mass (CoM) of the rear body  $G_r$ . The IMU measures the angular velocity  $\boldsymbol{\omega}^{G_r}$  acceleration  $\boldsymbol{a}^{G_r}$  in the rear body frame  $\mathfrak{R}_{G_r}$ . Assume that the IMU module is programmed with an *Attitude Heading and Reference System* (AHRS) sensor fusion algorithm which outputs the roll  $\phi$ , pitch  $\theta$  and yaw  $\psi$  angles of  $G_r$ . Note that we make a distinction between the roll and lean: The roll is a rotation about the  $x$ -axis of a frame that has previously been rotated about the local  $z$  and  $y$ -axes by the yaw and pitch respectively. In contrast, the lean is a rotation about the  $x$ -axis of  $\mathfrak{R}_V$ .

Lastly, assume that the *steer* angle of the steering head is measured with an encoder that also provides its time derivative the *steer rate*. Steer measured in the front body frame  $\mathfrak{R}_{G_f}$  is denoted by  $\delta$ . The projection of this

steer onto the road surface is denoted by  $\Delta$  and is expressed in  $\mathfrak{R}_V$ . The point  $V$  is the projection of  $G_r$  onto the road surface and its frame  $\mathfrak{R}_V$  is orthogonal to the road while translating with the motorcycle.

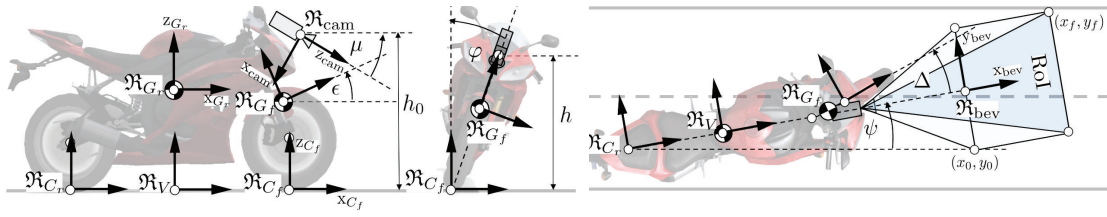


**Figure 2. Illustration of the proposed motorcycle-IMU-camera setup**

We adopt the following terminology when referring to the motorcycle geometry: The angle through which the front body is rotated with respect to the road normal is the *caster* angle  $\epsilon$ . The horizontal distance in  $\mathfrak{R}_{G_f}$  from the front wheel center to the motorcycle steering axis is the *rake*  $l_{rk}$ . The camera is rotated by a static pitch  $\mu$  in  $\mathfrak{R}_{G_r}$ , so that the road ahead dominates its *Field of View* (FoV).

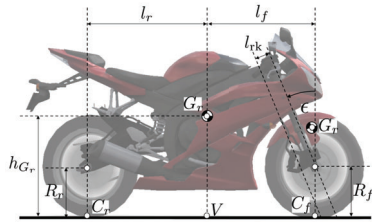


**Figure 3. Geometric parameters of the P2WV**

## FEATURE DETECTION & MATCHING

We define *features* as regions within at least two images of the same scene which could be recognized by a computer vision algorithm. Points, corners or patterns strongly contrasting with their environment make good feature candidates. Road scenes have been challenging for feature detection due to their relative homogeneity. However, digital camera resolutions and embedded processing power have improved at a geometric rate since the early development of computer vision in the 1980s. Hence, we hypothesize that it is now possible to capture enough detail of surface flaws present on roads to robustly extract features. Theoretically, the feature detection ought to work even better on roads with deteriorated lane markings and where the road surface has become potted over time.

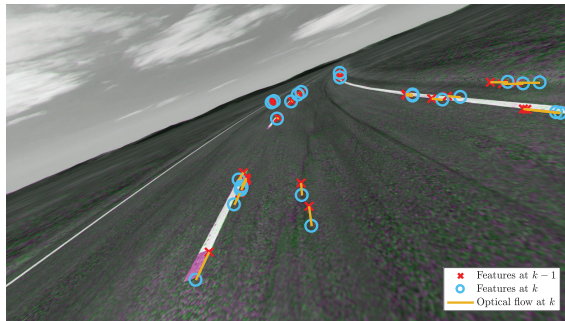


**Figure 4. Superimposed image pair taken at timesteps  $k - 1$  and  $k$ . Overlaid are the locations of the detected features at the respective time steps and the optical flow vectors between them.**

The Harris corner detector [15] is one of the earliest developed robust feature detection algorithms. Consider a small  $n \times n$  window of pixels  $W$  in a grayscale image  $I$ . A given  $W$  is considered a corner if displacing the window in any direction always results in a large change in the intensity gradient. Passing this window over the entire

image produces a map of corner features. Referring to Algorithm 1, the implementation is as follows: For every pixel  $I(x, y)$ , compute the image gradients in the  $x$  and  $y$  directions  $I_x$  and  $I_y$  of the window  $W$  surrounding it. Here, we calculate the gradients by convolving with the Sobel kernels  $G_x$  and  $G_y$ . Construct the structure tensor  $M$  from these and compute the *cornerness* score  $R$  for each pixel. A higher score indicates the presence of a corner. Finishing steps for the algorithm typically include thresholding  $R$  for higher scores followed by non-maximum suppression. There are many more modern feature detectors such as the Scale-Invariant Features Transform (SIFT) and the Features from Accelerated Segment Test (FAST). While we may choose to implement one of these in our approach at a later date, a comparison of feature detectors is not the focus of this work.

---

**Algorithm 1** The Harris corner detector

---

```

function HARRISCORNERS( $I, n$ )
   $G_x \leftarrow [1 \ 2 \ 1]^T * [1 \ 0 \ -1]$ 
   $G_y \leftarrow [1 \ 0 \ -1]^T * [1 \ 2 \ 1]$ 
   $w \leftarrow \frac{1}{2} [-n..n]$ 
   $\kappa \in [0.04, 0.06]$ 
  for all  $x \in I$  do
    for all  $y \in I$  do
       $W \leftarrow I(x + w, y + w)$ 
       $I_x \leftarrow G_x * W$ 
       $I_y \leftarrow G_y * W$ 
       $M \leftarrow \sum_{(x,y) \in W} \begin{bmatrix} I_x^2 & I_x I_y \\ I_x I_y & I_y^2 \end{bmatrix}$ 
       $R(x, y) \leftarrow \det M - \kappa (\text{tr } M)^2$ 
    end for
  end for
  return  $R$ 
end function

```

---

The next task is to identify matching features between sequential video frames of the road. We convert each feature pixel window into a *binary descriptor* which describes differences in intensity values in the window. Descriptors have the advantage of simplifying the matching process into thresholding the Hamming distance between two binary strings. Popular descriptor schemes include Binary Robust Independent Elementary Features (BRISF) and Binary Robust Invariant Scalable Keypoints (BRISK). For this work, we chose the widely-used Fast Retina Keypoint (FREAK) [16].

## INVERSE PERSPECTIVE MAPPING

The positions of the features detected in Section are expressed in a *perspective projection* of the world frame  $\mathfrak{R}_w$  at this stage. Furthermore, these positions are given in pixels rather than meters. IPM constructs a synthetic Bird’s Eye View (BEV) from an image taken in perspective. Consider a rectangular *Region of Interest* (RoI) in the real world we wish to view from above defined by corner points  $\mathbf{p}_0$  and  $\mathbf{p}_f$  in meters as shown in Figure 2. We convert these corner points into *homogeneous coordinates*  $\tilde{\mathbf{p}}_0$  and  $\tilde{\mathbf{p}}_f$  through division by the camera height.

$$\tilde{\mathbf{p}}_i = \begin{bmatrix} \frac{1}{h} \mathbf{p}_i^T & 1 \end{bmatrix}^T \quad (8)$$

We infer the existence of a *virtual camera* looking down from above at the RoI of resolution  $m_{VC} \times n_{VC}$ . The pixel intensity values in the images taken by the real camera and those taken by the virtual camera are related by a *Homography* matrix  $\mathbf{H}$  [17].

$$\mathbf{H} = \mathbf{K} \left( \mathbf{R}_{VC} - \frac{1}{h} \mathbf{t} \mathbf{n}^T \right) \mathbf{K}_{VC}^{-1} \quad (9)$$

Where  $\mathbf{R}_{VC}$  is the rotation matrix defining the orientation of the virtual camera VC with respect to the real one.  $\mathbf{t}$  is the displacement of the virtual camera with respect to the real camera and  $\mathbf{n}$  is the unit normal to the road surface.  $\mathbf{K}$  and  $\mathbf{K}_{VC}$  are the *intrinsic parameter matrices* of the real and virtual cameras respectively. We can approximate the inverse of the virtual camera intrinsic matrix by expressing the desired size of each of the pixels in the BEV in world coordinates [6].

$$\mathbf{K}_{VC}^{-1} = \begin{bmatrix} \frac{\tilde{x}_f - \tilde{x}_0}{m_{VC}} & 0 & -\tilde{x}_f \\ 0 & \frac{\tilde{y}_f - \tilde{y}_0}{n_{VC}} & -\tilde{y}_f \\ 0 & 0 & 1 \end{bmatrix} \quad (10)$$



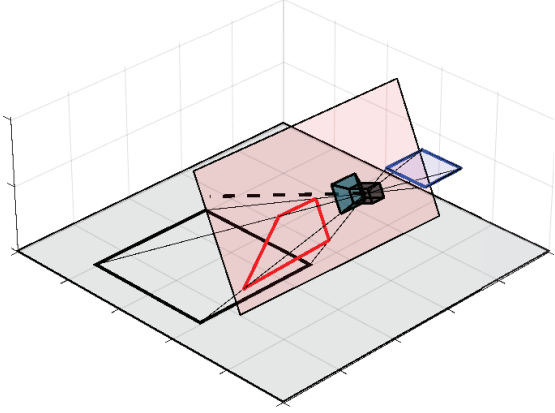


**Figure 5. Geometry of the IPM process.** First, we define a plane for the BEV (highlighted in blue above) in world frame units. Next, we project this plane onto the camera image plane (highlighted in red). Thus, it becomes our region of interest in the real world (highlighted in black)

Now, we define the orientation of the real camera with respect to VC. Note that in Figure 2 that the real camera  $z$ -axis is colinear with the axis of the focal point. First, we re-orient the camera axes so that it is the  $x$ -axis instead which projects forwards using  $\mathbf{R}_c$ .

$$\mathbf{R}_c = \mathbf{R}_y(\pi/2)^T \mathbf{R}_x(\pi/2) \quad (11)$$

Next, we undo the rotation by the tilt so that the camera position is expressed in the motorcycle body frame  $\mathfrak{R}_{G_r}$ . Finally, VC yaws with the motorcycle so we need to undo only the roll followed by the pitch to arrive in  $\mathfrak{R}_V$ , the reference frame in which the position of the virtual camera is defined.

$$\mathbf{R}_{VC} = \mathbf{R}_c (\mathbf{R}_\theta \mathbf{R}_\phi \mathbf{R}_\mu)^T \quad (12)$$

We form the intrinsic matrix  $\mathbf{K}$  of the real camera using its focal length  $f$  and the pixel size  $m_x \times m_y$ . The translations  $t_x$  and  $t_y$  compensate for the difference in coordinate origins between an image, where the origin is the top left corner, and the BEV, where the origin is at the bottom center.

$$\mathbf{K} = \begin{bmatrix} fm_x & 0 & m_x t_x \\ 0 & fm_y & m_y t_y \\ 0 & 0 & 1 \end{bmatrix} \quad (13)$$

Finally, we construct the homography matrix  $\mathbf{H}_{VC}$ . Note that there is no translation: Figure 5 shows that in reality IPM is a *warping* of the RoI in perspective as if the real camera were orthogonal to the world plane facing down, thus the translation is implicitly incorporated into the design of the  $\mathbf{K}_{VC}$ .

$$\mathbf{H}_{VC} = \mathbf{K} \mathbf{R}_{VC} \mathbf{K}_{VC}^{-1} \quad (14)$$

Recall the use of homogeneous coordinates in (8): A point  $\mathbf{p}_{im}$  in the original image (in pixels) is expressed in the BEV as  $\mathbf{p}_{bev}$  using the *inhomogeneous* form of the projective transform where  $h_{i,j}$  is an element of  $\mathbf{H}$  located at row  $i$  and column  $j$ .

$$x_{bev} = \frac{h_{11}x_{im} + h_{12}y_{im} + h_{13}}{h_{31}x_{im} + h_{32}y_{im} + h_{33}} \quad (15)$$

$$y_{bev} = \frac{h_{21}x_{im} + h_{22}y_{im} + h_{23}}{h_{31}x_{im} + h_{32}y_{im} + h_{33}} \quad (16)$$

Having removed the perspective warp from the feature set, we can convert each feature point  $\mathbf{p}_i^V$  from pixels into meters by multiplying each feature by the inverse of the virtual camera intrinsic matrix to obtain our point sets on the road surface expressed in  $\mathfrak{R}_V$ .

$$\mathbf{p}^V = \mathbf{K}_{VC}^{-1} [x_{bev} \quad y_{bev} \quad 1]^T \quad (17)$$

An example of a perspective-corrected point set superimposed onto a synthetic BEV created using IPM and bilinear interpolation is shown in Figure 6. Note that this entire process is reversible by simply multiplying the perspective-corrected points by the inverse of  $\mathbf{H}$ .

## POINT SET REGISTRATION

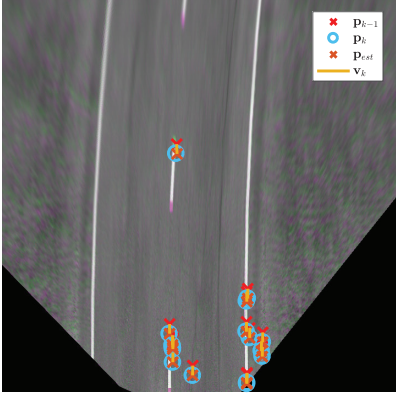


Figure 6. Features transformed into the planar coordinates. Note this time that the motions indicated in yellow are the calculated translational velocities from the ICP and not the optical flow.

Image registration is the process of determining the *affine* transformation between two images of the same scene. Thanks to the IPM, the registration problem here is restricted to two dimensions. We assume that the camera and IPM induce no distortion in the BEV, hence there exists a *rigid transformation* that optimally aligns the perspective-corrected point sets  $\mathbf{P}_k$  and  $\mathbf{P}_{k-1}$ . Let this transformation be composed of a rotation  $\mathbf{R}_\vartheta \in \mathbb{R}^{2 \times 2}$  about the virtual camera focal axis by  $\vartheta$  and a translation  $\mathbf{d} \in \mathbb{R}^2$  [18].

$$\begin{bmatrix} \mathbf{P}_{k-1} \\ \mathbf{I} \end{bmatrix} = \begin{bmatrix} \mathbf{R}_\vartheta & \mathbf{d} \\ \mathbf{0} & \mathbf{0} \end{bmatrix} \begin{bmatrix} \mathbf{P}_k \\ \mathbf{I} \end{bmatrix} \quad (18)$$

However, it is never the case that the features in image  $k - 1$  are a perfect rigidly transformed copy of those in image  $k$ , but a close approximation can be found using algorithms such as Iterative Closest Point. There exist several variations of ICP including such as point to point, point to plane and generalized ICP. Each of these minimizes a slightly different metric and vary in terms of robustness against the presence of outliers. In all cases though, ICP seeks to minimize the overlap error  $\mathbf{E}$  between point sets in the least-squares sense [19].

$$\min \sum_{k=1}^n \frac{1}{n} \|\mathbf{E}\|^2 = \sum_{k=1}^n \frac{1}{n} \|\mathbf{P}_{k-1} - \mathbf{R}_\vartheta \mathbf{P}_k - \mathbf{d}\|^2 \quad (19)$$

While iterative least-squares algorithms are more robust to outliers, this work is intended as a proof of concept rather than a final implementation. Thus, we select the well-known Singular Value Decomposition (SVD) variant of ICP summarized in Algorithm 2: First, center both point sets on zero by subtracting their means. Next, form the structure tensor  $\mathbf{A}$  from these centered sets and take its SVD. Verify that the product of  $\mathbf{U}$  and  $\mathbf{V}^T$  is orthogonal and multiply the end column by -1 if necessary. Finally, recover the translation using the difference between  $\mathbf{P}_{k-1}$  and the rotation-corrected  $\mathbf{P}_k$ .

---

### Algorithm 2 The Iterative Closest Point algorithm

---

```

function ICP( $\mathbf{P}_{k-1}, \mathbf{P}_k$ )
   $\mathbf{A} \leftarrow [\mathbf{P}_{k-1} - \bar{\mathbf{P}}_{k-1}] [\mathbf{P}_k - \bar{\mathbf{P}}_k]^T$ 
   $\mathbf{U}, \Sigma, \mathbf{V}^T \leftarrow \text{svd } \mathbf{A}$ 
  if  $\det \mathbf{R} = -1$  then
     $\mathbf{R} \leftarrow \begin{pmatrix} 1 & 0 \\ 0 & -1 \end{pmatrix} \mathbf{R}^T$ 
  end if
   $\mathbf{R} \leftarrow \mathbf{U} \mathbf{V}^T$ 
   $\vartheta \leftarrow \arctan \left( \frac{\hat{\mathbf{i}}^T \mathbf{r}_3}{\hat{\mathbf{k}}^T \mathbf{r}_3} \right)$ 
   $\mathbf{d} \leftarrow \bar{\mathbf{P}}_{k-1} - \mathbf{R} \bar{\mathbf{P}}_k$ 
  return  $\vartheta, \mathbf{d}$ 
end function

```

---

It is worth mentioning that the rotation between successive images  $k - 1$  and  $k$  can also be recovered from the IMU yaw rate measurement  $\tau\dot{\psi}$  where  $\tau$  is the system sample time [20].

## MOTORCYCLE KINEMATICS

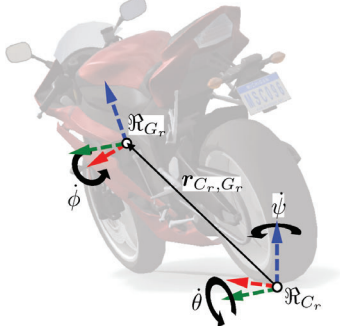


Figure 7. illustration of the relationship between the rear body center of mass and the rear wheel contact point

We assume that the translational velocity estimate from Section is measured in  $\mathfrak{R}_V$ . Let us approximate the motorcycle wheels as thin disks: Referring to Figure 7 and applying the rotations in the correct order, we obtain  $\mathbf{R}_{\theta\phi}$ , the rotation matrix transforming from  $G_r$  to  $C_r$ . From Screw theory, we know that the *twist* of a point  $i$  on a rigid body comprised of a translational velocity  $\mathbf{v}_i^b$  and an angular velocity  $\boldsymbol{\omega}^b$  can be expressed in the world frame  $\mathfrak{R}_w$  using the *velocity adjoint mapping*. Note that there also exists an inverse mapping to convert from the world frame back into the body frame.

$$\begin{bmatrix} \mathbf{v}_i^w \\ \boldsymbol{\omega}^w \end{bmatrix} = \begin{bmatrix} \mathbf{R}_b^w & [\mathbf{p}_i]_{\times} \mathbf{R}_b^w \\ \mathbf{0} & \mathbf{R}_b^w \end{bmatrix} \begin{bmatrix} \mathbf{v}_i^b \\ \boldsymbol{\omega}^b \end{bmatrix} \quad (20)$$

$$\begin{bmatrix} \mathbf{v}_i^b \\ \boldsymbol{\omega}^b \end{bmatrix} = \begin{bmatrix} \mathbf{R}_w^b & -\mathbf{R}_w^b [\mathbf{p}_i]_{\times} \\ \mathbf{0} & \mathbf{R}_w^b \end{bmatrix} \begin{bmatrix} \mathbf{v}_i^w \\ \boldsymbol{\omega}^w \end{bmatrix} \quad (21)$$

Recall from the system description that the IMU measures  $\boldsymbol{\omega}_{G_r}$  at  $G_r$  in  $\mathfrak{R}_{G_r}$ . With this in mind, we apply the Adjoint maps to express the ICP velocity estimate from the Section in  $\mathfrak{R}_{G_r}$ .

$$\begin{bmatrix} \mathbf{v}_{G_r}^{C_r} \\ \boldsymbol{\omega}_{G_r}^{C_r} \end{bmatrix} = \begin{bmatrix} \mathbf{R}_{\theta\phi}^T & -\mathbf{R}_{\theta\phi}^T [\mathbf{r}_{G_r, C_r}^{C_r}]_{\times} \\ \mathbf{0} & \mathbf{R}_{\theta\phi}^T \end{bmatrix} \begin{bmatrix} \mathbf{v}_{G_r}^{C_r} \\ \boldsymbol{\omega}_{G_r}^{C_r} \end{bmatrix} \quad (22)$$

$$= \begin{bmatrix} \mathbf{R}_{\theta\phi}^T & \mathbf{I} \\ \mathbf{0} & \mathbf{I} \end{bmatrix} \begin{bmatrix} \mathbf{v}_{G_r}^{C_r} \\ \boldsymbol{\omega}_{G_r}^{C_r} \end{bmatrix} \quad (23)$$

Next, we must derive the velocity of  $V$  to express the measured velocity at the front and rear contact points. This time applying the forwards Adjoint mapping, we obtain the following:

$$\begin{bmatrix} \mathbf{v}_V^V \\ \boldsymbol{\omega}^V \end{bmatrix} = \begin{bmatrix} \mathbf{R}_{\theta\phi} & [\mathbf{r}_{G_r, V}^{G_r}]_{\times} \mathbf{R}_{\theta\phi} \\ \mathbf{0} & \mathbf{R}_{\theta\phi} \end{bmatrix} \begin{bmatrix} \mathbf{v}_{G_r}^{C_r} \\ \boldsymbol{\omega}_{G_r}^{C_r} \end{bmatrix} \quad (24)$$

Finally, we obtain the front and rear slip angles from the  $x$  and  $y$  components of  $\mathbf{v}_V^V$  and the application of Equations (6) and (7). As discussed in the introduction, the leaning motion of the motorcycle means that the yaw rate is not equal to the angular velocity about the  $z$ -axis of  $\mathfrak{R}_{G_r}$ . However, it can be recovered through the orientation with respect to the road plane and the application of the proper *Rate Jacobian*.

$$\begin{bmatrix} \dot{\phi} \\ \dot{\theta} \\ \dot{\psi} \end{bmatrix} = \begin{bmatrix} 1 & 0 & -\sin(\theta) \\ 0 & \cos(\phi) & \sin(\phi)\cos(\theta) \\ 0 & -\sin(\phi) & \cos(\phi)\cos(\theta) \end{bmatrix}^{-1} \boldsymbol{\omega}_{G_r} \quad (25)$$

Note that due to the thin disk approximation, we expect to over-estimate the velocity somewhat compared to the ground truth as in reality  $r_{C_r, G_r}$  will not remain constant due to tire compression during transient phases.

## SENSOR FUSION

The estimator described thus far is summarized in Figure 8: The IMU consisting of a MEMS accelerometer and gyroscope feeds its readings to a standard INS, which outputs roll, pitch and the derivative of body velocity  $\dot{\mathbf{v}}_{G_r}^{G_r}$ . The camera feeds images to Algorithm 1 which outputs features to the IPM. From here, the ICP computes the motion between point sets and provides a planar velocity and yaw rate estimate. The planar velocity is converted into body velocity using the gyroscope measurement and the Adjoint mapping (22). Finally, the integrated INS velocity estimate is corrected for integrator drift using the vision estimate within the Kalman Filter. The velocity is fed back into the INS and the algorithm repeats for all time steps  $k$ .

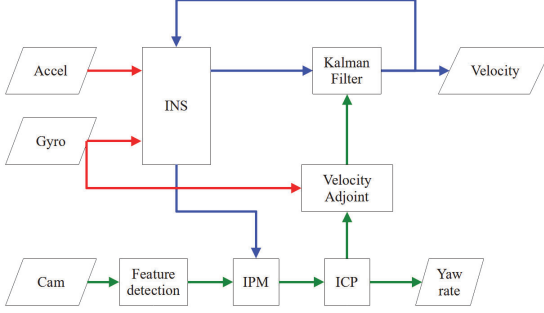


**Figure 8.** The proposed visual-inertial estimation algorithm: Measurements from the IMU sensors are highlighted in red. Readings from the proposed vision component are highlighted in green. State estimates are highlighted in blue.

We model noise present in the vision measurement as Average White Gaussian Noise (AWGN). We use a discrete *Linear Time-Invariant* (LTI) Kalman filter to produce an estimate of the motorcycle velocity  $v_{G_r}^{G_r}$ . Our prediction model is a simple integration on the input  $\dot{v}_{G_r}^{G_r}$  provided by the INS.

$$\mathbf{x} = [v_x^{G_r} \quad v_y^{G_r}]^T \quad (26)$$

$$\mathbf{u} = [\dot{v}_x^{G_r} \quad \dot{v}_y^{G_r}]^T \quad (27)$$

$$\mathbf{F} = \begin{bmatrix} 1 & 0 \\ 0 & 1 \end{bmatrix} \quad (28)$$

$$\mathbf{B} = \begin{bmatrix} \tau & 0 \\ 0 & \tau \end{bmatrix} \quad (29)$$

Where  $\mathbf{x}$  and  $\mathbf{u}$  denote the state and input vectors. Concordantly,  $\mathbf{F}$  and  $\mathbf{B}$  are the state and input transition matrices. Let  $\mathbf{P}$  and  $\mathbf{Q}$  be the error and process noise covariance matrices. The *prediction* equations are summarized below where the superscript  $-$  denotes an *a priori* state or covariance estimate.

$$\hat{\mathbf{x}}_k^- = \mathbf{F}\hat{\mathbf{x}}_{k-1}^- + \mathbf{B}\mathbf{u}_k \quad (30)$$

$$\mathbf{P}_k^- = \mathbf{F}\mathbf{P}_{k-1}^-\mathbf{F}^T + \mathbf{Q} \quad (31)$$

Referring to Figure 8 we apply (22) to the translational velocity measured by our vision algorithm to obtain our Kalman filter measurement. We summarize our measurement model below where  $\mathbf{z}$  is the measurement vector and  $\mathbf{H}$  is the measurement model.

$$\mathbf{z} = [v_x^{\text{ICP}} \quad v_y^{\text{ICP}}]^T \quad (32)$$

$$\mathbf{H} = \begin{bmatrix} 1 & 0 \\ 0 & 1 \end{bmatrix} \quad (33)$$

We complete the *update* step of Kalman filtering by computing the Kalman gain  $\mathbf{K}$  and the *a posteriori* estimate and covariance matrix. Note that  $\mathbf{R}$  is the measurement covariance matrix.

$$\mathbf{K}_k = \mathbf{P}_k^- \mathbf{H}^T (\mathbf{H} \mathbf{P}_k^- \mathbf{H}^T + \mathbf{R})^{-1} \quad (34)$$

$$\hat{\mathbf{x}}_k = \hat{\mathbf{x}}_k^- + \mathbf{K}_k (\mathbf{z}_k - \mathbf{H} \hat{\mathbf{x}}_k^-) \quad (35)$$

$$\mathbf{P}_k = (\mathbf{I} - \mathbf{K}_k \mathbf{H}) \mathbf{P}_k^- \quad (36)$$

## RESULTS

To validate our approach, we designed three scenarios in BikeSim mechanical simulation software. BikeSim allows developers to test their ARAS designs on realistic multi-body simulations of motorcycles. We tested our vision algorithm on three different driving scenarios. The first scenario sees the motorcycle perform a series of *slaloms* along a straight road at 50 km/h. This scenario was selected in order to test our estimator at high values of steering angle. The second scenario sees the motorcycle negotiate an S-shaped bend at 80 km/h. We chose this scenario to test our estimator's ability to cope with curved roads as well as straights. The third is the *Double Lane-Change* (DLC) often featured in literature where the motorcycle changes from one lane to another and back again on a straight road. We perform the DLC at 110 km/h. Here, the scenario was chosen in order to test the

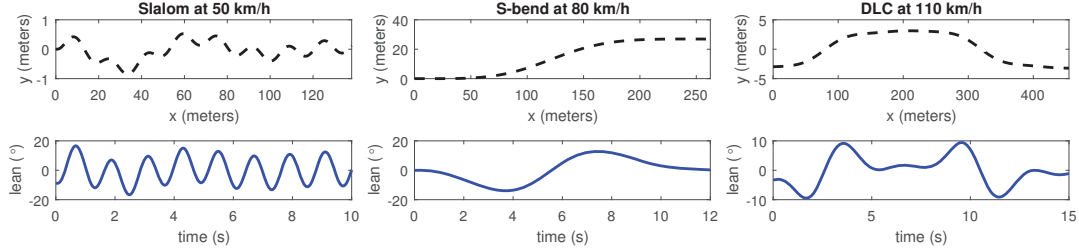


**Figure 9. Trajectory and lean profiles of the three scenarios**

algorithm’s ability to cope with elevated speeds typically experienced by riders on European extra-urban roads. The paths and lean profiles of each scenario are illustrated in Figure 9.

We implemented our estimator in MATLAB/Simulink in co-simulation with BikeSim at a sampling rate of 60 Hz. The outputs from the camera were  $720 \times 1280$  RGB images. We defined our RoI with corner points  $(x_0, y_0) = (3\text{ m}, -10\text{ m})$  and  $(x_f, y_f) = (23\text{ m}, 10\text{ m})$  in  $\mathfrak{R}_V$ . The BEV resolution was  $720 \times 720$  and we added noise to the accelerometer reading  $\mathbf{a}_{G_r}^{\text{accel}}$  with a Signal to Noise Ratio SNR = 30 to test our estimator’s robustness to integrator drift. The process and measurement covariance matrices were set to  $\mathbf{Q} = 1$  and  $\mathbf{R} = 1 \times 10^5$ .

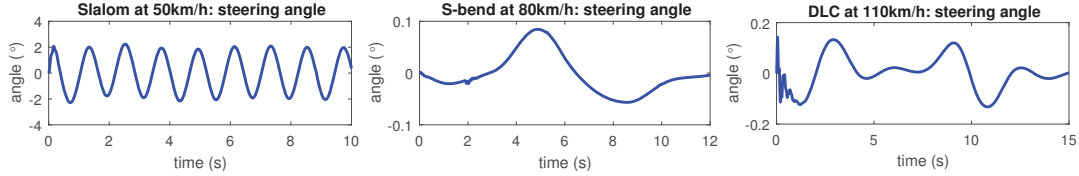


**Figure 10. Steering angle inputs for each scenario**

The following subsections present the results of the estimates obtained presented against ground truth references generated in BikeSim. In Figures 11, 12 and 13, the acronyms ICP, DR, and KF denote Iterative Closest Point, Dead-Reckon (of the INS velocity rate estimate) and Kalman Filter respectively.

### Longitudinal Velocity

We observe from Figure 11 that the ICP estimate rests around the reference value, if not slightly underestimating. This is an encouraging result as other estimation algorithms such as Optical Flow fail to register large displacements between images which is not the case here. However, in the Slalom scenario, the variance is much higher compared to the S-bend and DLC.

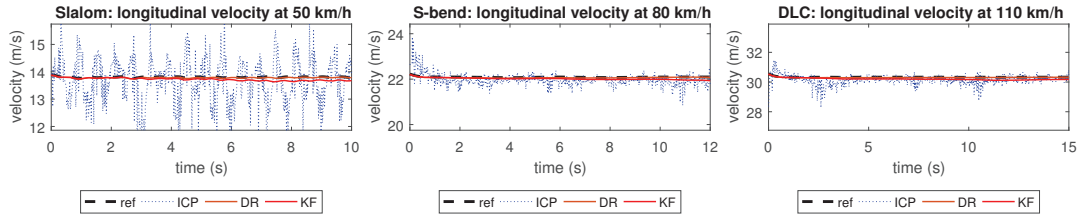


**Figure 11. Longitudinal velocity results**

### Lateral Velocity

Recall from the motivation that a key technical goal for our estimator is the reconstruction of the lateral velocity. The results displayed in Figure 12 are encouraging: We note that in the Slalom scenario, the vision system struggles to keep pace with the rapid succession of transients. However, this is compensated for by the INS measurement where integrator drift is less of an issue due to the rapidly-varying input. We observe that the both the INS and vision measurements track the reference very well in the S-Bend scenario.

Finally, we note that in the DLC the ICP estimate deviates slightly from the reference especially during transients corresponding to sudden changes in lean (see Figure 9). In all cases, we note that the integrated INS alone slowly drifts from the reference as the errors from the noise added to the accelerometer reading accumulate. As hypothesized, our vision algorithm measurement successfully compensates for this drift and drags the filtered estimate back toward the ground truth.

### Yaw Rate

So far, there has been significant noise present in all the ICP estimates obtained. It is clear from Figure 13 that this noise is especially present in the yaw rate estimate obtained from the estimated rotation matrix in

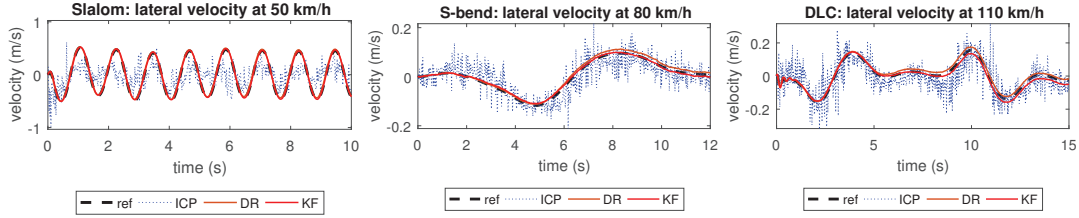


Figure 12. Lateral velocity results

Algorithm 2. While the mean of this noise appears to track the reference well, we note in the S-bend and DLC scenarios that there is slight overshoot at the peaks of motion.

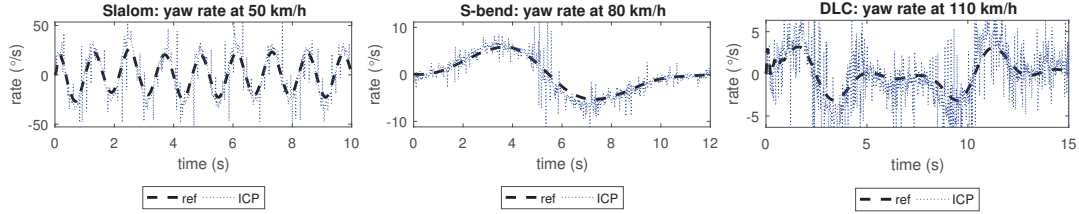


Figure 13. Yaw rate results

### Front Slip

Having obtained our velocity estimates, we re-express them in  $\mathfrak{R}_V$  using (24) and pass the results to (6) and (7). It should be noted that these expressions for front and rear slip are themselves linearized approximations of the ground truth therefore there is an upper bound on achievable performance. Recall that a front slip larger than the rear slip indicates under-steering: We observe from Figure 14 good tracking in the Slalom scenario where front slip is highest. Note also from the steering inputs in Figure 10. that the majority of the angle between direction and velocity in  $\mathfrak{R}_{C_f}$  is due to the steering angle. We note an underestimation in the S-bend and DLC.

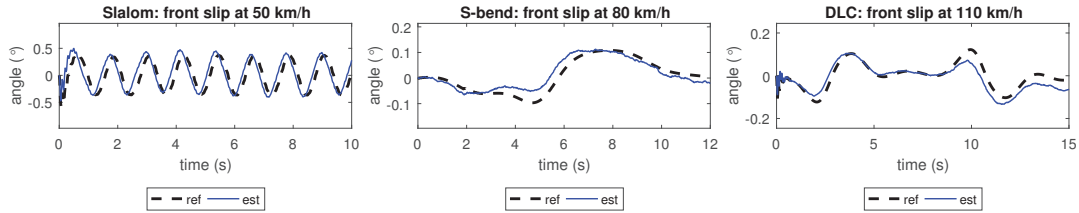


Figure 14. Front slip results

### Rear Slip

The results for the rear slip angle are displayed in Figure 15. The S-bend and DLC estimates track much better than their front slip counterparts though we note that the magnitude of the references here are more significant. We observe that the estimate lags in the Slalom scenario.

## DISCUSSION

The initial evaluation of our results is encouraging. Referring to Figures 12 we note that our results compare favorably with the Kalman-based approach of Teerhuis and Jansen [21] despite there being no a priori model in our estimator. Regarding performance against observer-based designs, note that the estimate during the peak regions of the DLC outperforms the estimation by the UI-HOSM [11] while performing the same maneuver. This comparison is of particular importance since the results in [11] were also obtained using BikeSim. Recall that in [22], the absolute error magnitude in their observer lateral velocity estimation during a DLC using a nominal LPV model was just over 0.12 m/s. We note an error in our DLC result of under 0.05 m/s, outperforming that paper’s LPV observer. Of particular importance is that while the control inputs of the scenarios in [22] are generated using BikeSim, they are validated against a theoretical model. Thus, we can conclude that our estimator outperforms theirs even in the best case. In [13], a highly sophisticated multi-model observer based on Tagaki-Sugeno and *Linear Matrix Inequalities* (LMI) techniques is presented and demonstrates the most promising results for observer-based lateral velocity estimates to date. While their observer does reach the correct final value in steady-state periods, it fails to reconstruct the waveforms of transients compared to our approach.

In the Motivation, we mentioned that longitudinal velocity can be recovered from the vehicle engine odometer under the assumption that no longitudinal slip is present between the road and the tires. This is nevertheless a harsh assumption to make, especially in road conditions where such slip is likely to be present such as wet

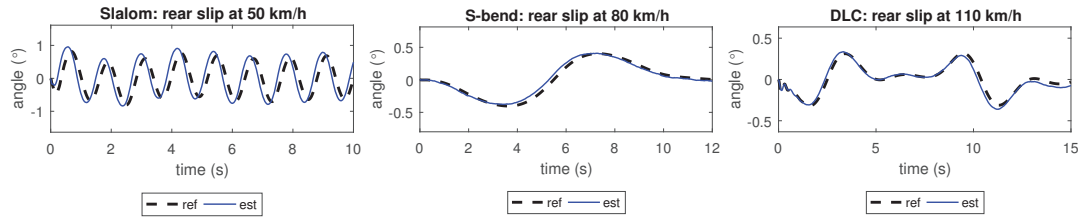


Figure 15. Rear slip results

weather. For this work, we chose to work with constant longitudinal velocities since the primary motivation is to reconstruct lateral motion and the front and rear slip angles. Future works on our algorithm should test its ability to estimate a varying longitudinal velocity.

Earlier works published by our research team attempted to measure lateral velocity using only information from BEV images of the center lane markers [23]. We identified two major issues with this approach which in part motivated this new design: The sudden appearance and removal of transitioning lane markers entering the BEV induced a large-amplitude low-frequency oscillation in the vision system measurement. We have overcome this by using road surface detailing as tracked features as well as lane markers as explained in Section . The second major issue was computational complexity: Producing a full grayscale BEV using image interpolation is extremely intensive for any application. We proposed to reduce complexity through image binarization. However, this introduced a new source of noise into our measurement. Here, we transform only the features detected in the camera images into the inverse perspective, greatly reducing computational complexity whilst simultaneously decreasing noise.

Nonetheless, there is strong noise present in all of our ICP measurements originating outside of the sources discussed. A known issue with point registration is how one deals with *outliers*. A common technique is to detect them using Random Sample Consensus (RANSAC) [24]: Future works on this approach should investigate the influence of outliers on our results. We are also limited by the BikeSim software itself as the simulated IMU readings from the physics engine and the simulated image stream from the visualizer are asynchronous. This leads to imperfect IPM, especially at high roll angles and we hypothesize that this is the cause of the deviations from the ground truth observed in Figures 12 and 13. It may be possible to reduce measurement noise by increasing the sample rate of the video stream and the resolution of the camera.

As mentioned in the front slip results, there is an upper limit to the possible accuracy of the slip estimates using (6) and (7). Nevertheless, our estimates do approximate the transient behavior well if under-estimating their magnitude. It would be worthwhile in future works to implement our estimator in its current form as an ARAS to detect critical steering scenarios and test it against simulations of motorcycle crashes in BikeSim.

## CONCLUSIONS

In this article, we propose a method of estimating the velocity and wheel lateral slip angles of a motorcycle traveling at high speed along a single-carriageway road. We extract features from images captured by a camera fixed to the front of the motorcycle and use Harris corner detection to extract features. We remove the perspective projection from the point sets using IPM and recover ego-motion using Iterative Closest. Finally, we obtain a velocity estimate using sensor fusion with an Inertial Navigation System and a Kalman filter. We validated our approach against three different BikeSim simulation scenarios and compared the obtained results with other approaches. We conclude that our approach compares very well to the state of the art and surpasses it in a few cases. We recommend that future works should investigate the effects of outliers, sensor resolution and frame rate on the accuracy of our vision measurements. We will refine our algorithm in simulations under non-ideal conditions such as rain, poor marker visibility, and a rough road surface. Furthermore, we will perform tests under more diverse scenarios such as periods of longitudinal acceleration and simulated crashes. Eventually, we hope to validate our approach using real-world data from an experimental P2WV rig situated at IBISC.

## REFERENCES

- [1] ONSIR. Le parc automobile des ménages. resreport, Observatoire national interministériel de la sécurité routière, September 2021. URL <https://www.onisr.securite-routiere.gouv.fr/etudes-et-recherches/vehicules/parc-des-vehicules/le-parc-deux-roues-motorises-des-menages>.
- [2] Andrea D. Furlan, Tara Kajaks, Margaret Tiong, Martin Lavallière, Jennifer L. Campos, Jessica Babineau, Shabnam Haghzare, Tracey Ma, and Brenda Vrkljan. Advanced vehicle technologies and road safety: A scoping review of the evidence. *Accident Analysis & Prevention*, 147, 2020. ISSN 0001-4575. doi: 10.1016/j.aap.2020.105741.
- [3] Peter Corke. An inertial and visual sensing system for a small autonomous helicopter. *Journal of Robotic Systems*, January 2004. doi: 10.1002/rob.10127.

- [4] D. Ortín and J. M. M. Montiel. Indoor robot motion based on monocular images. *Robotica*, 19(3):331–342, 2001. doi: 10.1017/S0263574700003143.
- [5] Bojian Liang and N. Pears. Visual navigation using planar homographies. In *Proceedings 2002 IEEE International Conference on Robotics and Automation (Cat. No.02CH37292)*, volume 1, pages 205–210 vol.1, May 2002. doi: 10.1109/ROBOT.2002.1013362.
- [6] Pierre-Marie Damon, Hicham Hadj-Abdelkader, Hichem Arioui, and Kamal Youcef-Toumi. Inverse perspective mapping roll angle estimation for motorcycles. In *2018 15th International Conference on Control, Automation, Robotics and Vision (ICARCV)*, pages 349–354, November 2018. doi: 10.1109/ICARCV.2018.8581182.
- [7] Vittore Cossalter. *Motorcycle Dynamics*. Lulu, second edition, October 2006. ISBN 1430308613.
- [8] V. Cossalter, R. Lot, and M. Peretto. Steady turning of motorcycles. *Proceedings of the Institution of Mechanical Engineers, Part D: Journal of Automobile Engineering*, 221(11):1343–1356, 2007. doi: 10.1243/09544070JAUTO322.
- [9] CMC. Accurate localisation for motorcycles remains a challenge. Technical report, Connected Motorcycle Consortium, April 2019. URL <https://www.cmc-info.net/news/archives/04-2019>.
- [10] R. S. Sharp. The Stability and Control of Motorcycles. *Journal of Mechanical Engineering Science*, 13(5): 316–329, 1971. doi: 10.1243/JMES\_JOUR\_1971\_013\_051\_02.
- [11] Lamri Nehaoua, Dalil Ichalal, Hichem Arioui, Jorge Davila, Saïd Mammar, and Leonid M. Fridman. An unknown-input hosm approach to estimate lean and steering motorcycle dynamics. *IEEE Transactions on Vehicular Technology*, 63(7):3116–3127, September 2014. ISSN 1939-9359. doi: 10.1109/TVT.2014.2300633.
- [12] Pierre-Marie Damon. *Estimation pour le développement de systèmes d’aide à la conduite des véhicules à deux-roues motorisés*. Theses, Université Paris-Saclay ; Université d’Evry-Val-d’Essonne, November 2018. URL <https://hal.archives-ouvertes.fr/tel-02024804>.
- [13] M. Fouka, L. Nehaoua, H. Arioui, and S. Mammar. Interconnected observers for a powered two-wheeled vehicles: Both lateral and longitudinal dynamics estimation. In *2019 IEEE 16th International Conference on Networking, Sensing and Control (ICNSC)*, pages 163–168, May 2019. doi: 10.1109/ICNSC.2019.8743290.
- [14] P-M Damon, D. Ichalal, L. Nehaoua, H. Arioui, and S. Mammar. Rider weight consideration for observer design with an application to the estimation of the lateral motorcycle dynamics and rider’s action. In *2017 IEEE International Conference on Systems, Man, and Cybernetics (SMC)*, pages 3237–3242, 2017. doi: 10.1109/SMC.2017.8123127.
- [15] Chris Harris and Mike Stephens. A combined corner and edge detector. In *Proceedings of the Alvey Vision Conference*, 1988. doi: 10.5244/C.2.23.
- [16] Alexandre Alahi, Raphael Ortiz, and Pierre Vanderghenst. FREAK: Fast Retina Keypoint. In *2012 IEEE Conference on Computer Vision and Pattern Recognition*, pages 510–517, June 2012. doi: 10.1109/CVPR.2012.6247715.
- [17] Richard Hartley and Andrew Zisserman. *Multiple View Geometry in Computer Vision*. Cambridge University Press, second edition, 2004. ISBN 978-0-521-54051-3. doi: 10.1017/CBO9780511811685.
- [18] Y. Liu, T.S. Huang, and O.D. Faugeras. Determination of camera location from 2-d to 3-d line and point correspondences. *IEEE Transactions on Pattern Analysis and Machine Intelligence*, 12(1):28–37, January 1990. ISSN 1939-3539. doi: 10.1109/34.41381.
- [19] Fang Wang and Zijian Zhao. A survey of iterative closest point algorithm. In *2017 Chinese Automation Congress (CAC)*, pages 4395–4399, October 2017. doi: 10.1109/CAC.2017.8243553.
- [20] Pierre-Marie Damon, Majda Fouka, Hicham Hadj-Abdelkader, and Hichem Arioui. Vision-based lane crossing point tracking for motorcycles. In *2019 IEEE Intelligent Transportation Systems Conference (ITSC)*, pages 3399–3404, October 2019. doi: 10.1109/ITSC.2019.8917206.
- [21] A. P. Teerhuis and S. T. H. Jansen. Motorcycle state estimation for lateral dynamics. *Vehicle System Dynamics*, 50(8):1261–1276, 2012. doi: 10.1080/00423114.2012.656655.
- [22] P. M. Damon, H. Dabladji, D. Ichalal, L. Nehaoua, and H. Arioui. Estimation of lateral motorcycle dynamics and rider action with Luenberger observer. In *2016 IEEE 19th International Conference on Intelligent Transportation Systems (ITSC)*, pages 2392–2397, November 2016. doi: 10.1109/ITSC.2016.7795941.
- [23] Martin Pryde, Lamri Nehaoua, Hicham Hadj-Abdelkader, and Hichem Arioui. Visual-inertial lateral velocity estimation for motorcycles using inverse perspective mapping. In *The 17th International Conference on Control, Automation, Robotics and Vision (ICARCV 2022)*, December 2022.
- [24] Davide Scaramuzza. 1-point-RANSAC structure from motion for vehicle-mounted cameras by exploiting non-holonomic constraints. *International Journal of Computer Vision*, 2011. doi: 10.1007/s11263-011-0441-3.



## **Automatic Braking Systems and Blind Spot as Examples for New Approaches in Type Approval Regulations towards Robust Active Safety Systems**

**Patrick Seiniger**

German Federal Highway Research Institute (BASt)

Paper Number 23-0267

### **ABSTRACT**

Traditional type approval regulations typically define a small set of very precisely defined test cases that act as an implicit requirements definition. Especially for active safety regulations, this leads to two major problems: Firstly, the implicit requirements are given only for a small number of operating points, and secondly, the prescribed test cases will typically happen only on an ideal test track.

The newest type approval regulations, such as especially the new regulation on automated emergency braking systems for heavy vehicles, define requirements in a broader way over the whole operating range, in a certain range of parameters (such as: for centerline offsets between -20 and +20 cm) and leave provisions for technical services and/or market surveillance authorities to test in different, more realistic conditions. They also require the systems to not change strategy for cases out of the specifications (e.g.: for higher centerline offsets).

As a consequence, this shifts the specification responsibility away from the regulator, towards the vehicle manufacturer. In this way, there is more freedom of design while still maintaining an appropriate level of safety. Also, the verification task is shifted towards the technical service, who now has the responsibility to certify that the vehicle or system matches the given overall requirements by specific test cases. The market surveillance authority, however, has the freedom to check each and every aspect of the system against the requirements. Market surveillance therefore acts as a supervisor for the technical services.

In the proposed paper, this new approach is presented in detail with the examples of Regulation 131-02 (automated emergency braking for heavy vehicles) and Regulation 151 (blind spot information systems). The new approach is described in detail with examples from the regulation, as well as the necessary equipment to perform the test runs in the case of Regulation 151: driving robots, robot-controlled bicycle dummy etc. Finally, proposals will be given on how to judge whether a system complies with the requirement to not change strategy; a topic that will become relevant in the coming years.

The combination between broad requirements, not changing system strategy when out of the main operating range, vague defined test cases and market surveillance as a supervisor for technical services has the potential to make the type approval system fit for the future, and especially for all intelligent or flexible or programmable safety systems, on the one hand.

On the other hand, technical services will have to adapt to the new responsibility and manufacturers to the new flexibility, since the regulation now does not exactly specify (overspecify?) a safety system, but more specifies the expected risk balance. It will certainly take some time and discussions until the new approach will fully unfold its potential.

## INTRODUCTION

Flexible, programmable or intelligent (FPI) systems are a challenge for the traditional type approval regime: It is hard to define few worst case test cases with which the expected performance of those systems over the whole operating range can be verified, since there is not necessarily a strictly monotone dependency between test parameters and test outcome, like it in general is for classical mechanical systems, see example in Figure 1.

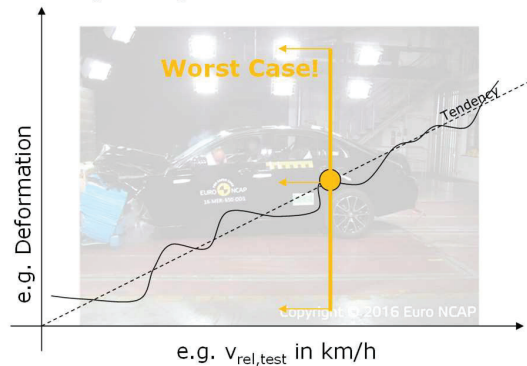


**Figure 1: Example for the tendency between test parameter ( $v_{rel,test}$ ) and test result (deformation)**

FPI systems in the type approval regime include advanced driver assistance systems, automated driving systems, but also emission-limiting systems, noise pollution prevention and others. This challenge was brought to the attention of the public in 2015 in the course of the emissions scandal where vehicles were designed to function during type approval procedures, but not in real driving conditions – in some cases a good example of test optimization, in other cases a breach of the rules.

A new approach for type approval helps to make the type approval system more robust against test optimization and make it effective also for FPI systems, which we will see in the future in more and more type approval disciplines.

## NEW REGULATION APPROACH VS. TRADITIONAL REGULATIONS

The new approach, as opposed to the traditional type approval regulation consists of four elements that help to overcome the weakness that comes with only a limited set of tests. A comparison for key elements of the new approach with traditional regulations is shown in Figure 1.

**Table 1: Comparison of new approach and traditional regulations**

Category	New approach	Traditional regulations
Requirements definition	Explicit, over the whole operating range, with interpolation tables, functions etc.	Implicit by expected test results, for representative test cases only
Performance off-cycle	Requirement to not change control strategy	-
Test case definition	Vague, As a guidance: other conditions can be tested as well, Expected test results given per reference to requirements	Precise, Test of other conditions not foreseen, Expected test results given with test definition
Number of test cases	Typically high number of test cases, procedure how to deal with failed tests	Typically low number of test cases
Surveillance system	Market surveillance, Conformity of Production	Conformity of Production

The differences with regard to these items will be explained in this section.

### Explicit vs. Implicit Requirements

Requirements are implicit if the requirements are not specified in general terms but result from the pass criteria of a limited test program. For this the precise description of the tests and the respective pass criteria is necessary.

With implicit specification, the system or vehicle to be tested can be regarded as a "black box" whose internal decision-making procedures are unknown. Verification by means of tests is therefore possible in principle even without manufacturer knowledge. Moreover, the method is easy to practice (tests are clearly predefined and do not have to be adapted to the specific product, the expected outcomes are clearly described as pass criteria). Typically, environment conditions for the test, such as weather, test surface,

vehicle configuration are exactly specified. The disadvantage of this method – important for robust driver assistance systems regulations – is that performance requirements for conditions other than the test conditions are not specified.

Thus, one approach that is becoming increasingly prevalent in more recent driver assistance regulation documents is the concrete, numerical or mathematical definition of verifiable requirements. These requirements - unless further restricted - apply comprehensively (for example: for all driving speeds, for all weather conditions, for all vehicle configurations and so on).

In many cases, the function fulfilment (example: emergency brake assist function) is neither physically nor technically possible in every situation. Comprehensible restrictions are then specified (in the example: definition of speed reduction for dry road surfaces).

#### **“Do Not Change Strategy” – Off-Cycle Performance Requirements**

Additionally, robust systems should try to do their best to avoid accidents, even outside of the range for which requirements are defined. Therefore, a typical requirement is that the corresponding function must not exhibit any unjustified switching of the control strategy even outside the restrictions.

#### **Vaguely Defined Test Cases for Explicit Requirements**

As stated above, traditional type approval regulations specify the tests very precisely. This ensures that the tests done by different technical services are comparable. However, this method does allow optimization for the test. A more important challenge is that for flexible, programmable and intelligent systems, the fact that tests in worst-case conditions are passed does not necessarily mean that test in other, non-worst-case conditions the tests are passed as well. For explicit requirements, it is not of great importance to exactly specify test conditions since the performance requirements are defined independent from test cases. Under some circumstances, it can be an advantage to only define tests very vaguely, allowing technical services and market surveillance authorities to explore the performance of the system over the whole operating range.

However, the effort required to test the requirements can increase considerably when applying this method, and the test cases will not necessarily be the same in number and parameters for each type approval test series. Moreover, in some cases, the tests that remain in the regulations are so vaguely defined that technical

services, type approval and market surveillance authorities must have a deep understanding of possible system limits (for example, in the application of UN Regulation No. 157 on automated lane-keeping systems).

Test definition will also allow testing of off-cycle performance (“do not change strategy”); in this case, identifying the expected performance is not trivial. A method for this is proposed below.

#### **Market Surveillance Process**

Previously, under the European Framework Directive 2007/46/EC, once a type approval had been granted by one member state of the EU, it could only be questioned and reviewed by another member state with high hurdles, the only quality control process over the lifetime of a product was the so-called “Conformity of Production”, where the conformance of the produced products with the type-approved products is checked. The new Framework Regulation (EC) No. 2018/858 introduces the system of so-called market surveillance. It now allows any vehicle type-approved granted on the basis of the Framework Regulation to be inspected by the market surveillance authorities of the member states or the Joint Research Center of the European Commission with regard to compliance with the requirements. It is not yet fully clear how exactly market surveillance will be implemented. However, it has the potential to fundamentally change the type approval system.

Without market surveillance, generically formulated test cases (example: "braking from any speed", as opposed to precisely specified test conditions "braking from X km/h with tolerance Y") could be a disadvantage, because it is then up to only one technical service and one type approval authority to verify compliance with the requirements, and this one technical service could possibly select parameter combinations that are particularly easy to meet without further specifications.

With market surveillance, generically formulated test cases are advantageous because not only the initial technical service and the approval-issuing authority check compliance with the requirements, but potentially many other member states can also do so on the basis of possibly completely different test cases. The vehicle manufacturer is therefore forced to design the system robustly. Optimization for the "one" test is no longer possible without the risk of sanctions.

This requires a rethink in the formulation of vehicle technology regulations towards the specification of generally valid requirements (especially in the case of driver assistance systems), which are not limited - as in the past - to a few requirements specified by

concrete test cases. The generally valid requirements can be verified by more and generically defined test cases. Because artificial target objects often used in tests can by their very nature never fully represent reality and can lead to malfunctions, this then also includes the creation of opportunities for retesting (in case of fails) on a limited scale with clear definition of criteria for test repetition.

## **IMPLEMENTATION IN REGULATIONS (UN) NO. 131-02 & 152, AUTOMATIC EMERGENCY BRAKING SYSTEMS**

An automatic emergency braking system regulation was amongst the first advanced driver assistance system regulation in the UN ECE framework. After a major overhaul, which resulted in the second series of amendments to Regulation (UN) No. 131 and pending modifications to Regulation (UN) No. 152, AEBs regulations are now amongst the most modern regulations. They showcase how the “new approach” as defined in the last section can be implemented. This will be discussed in the following section; text with grey background in this section is taken from Regulation 131-02 (document GRVA-12-50rev1).

### **Requirements Section**

The “new approach” starts with a formulation of verifiable requirements for the system. Verifiable requirements do not contain items like “long”, “small”, “short” etc., but contain concrete values. Regulation (UN) No. 131-02 [1] has the performance requirement for the automatic braking function in paragraph 5.2.1.4 (and some others for other AEB functions).

### **Performance Statement**

The paragraph starts with the statement that the required performance is stated for a set of conditions:

*5.2.1.4. Speed reduction by braking demand  
In absence of driver's input which would lead to interruption according to paragraph 5.3.2., the AEBs shall be able to achieve a relative impact speed that is less or equal to the maximum relative impact speed as shown in the following table, provided:*

A list of conditions follows that defines the boundary conditions for when the performance targets are required to be achieved. They are derived from the scope of the regulation (here: an assistance system that aids the driver, but is not able to avoid each and every accident automatically).

### **Environmental Conditions**

The conditions in the case of R131-02 are grouped into a list of four exhaustive items, starting with the

condition that the environmental conditions allow for maximum brake decelerations – which means that adoption of the control strategy to other conditions such as low friction is not required (which is different to regulations for automated driving systems such as R157 [2]). Note that this item, like almost all items, contains an exhaustive list as well.

*(a) Vehicle external influences allow for the required deceleration, i.e.:*

*(i) The road is flat, horizontal and dry affording good adhesion;*

*(ii) The weather conditions do not affect the dynamic performance of the vehicle (e.g. no storm, not below 0°C);*

Note that this looks like ideal conditions on the test track in the first place, but it requires the full performance also close to metal guardrails, sign posts, with lane markings and the like – since all these items are not excluded. This is a major step towards robustness of the regulation.

### **Vehicle Conditions**

The next group defines that the vehicle itself shall be able to achieve the required deceleration, giving examples, not an exhaustive list. The reasoning behind this is that the vehicle's possible deceleration can be impaired by improper maintenance and other facts not under the control of the vehicle manufacturer. An item to keep in mind for later discussions is the trailer under bullet (iv), which is typical for the operation of heavy vehicles.

*(b) The vehicle state itself allows for the required deceleration, e.g.:*

*(i) The tyres are in an appropriate state and properly inflated;*

*(ii) The brakes are properly operational (brake temperature, pads condition etc.);*

*(iii) There is no severe uneven load distribution;*

*(iv) No trailer is coupled to the motor vehicle and the mass of the motor vehicle is between maximum mass and mass in running order conditions;*

### **Perception Conditions**

While the upper two condition groups look at whether full deceleration is possible, AEBs systems also require the targets to be detectable. Some environment conditions, mainly water in the air, decrease the possible RADAR sensor performance, and bad visual conditions are a problem for camera sensors. This lead to the definition of the following conditions, again an exhaustive list:

*(c) There are no external influences affecting the physical sensing capabilities, i.e.:*

- (i) The ambient illumination conditions are at least 1000 Lux and there is no extreme blinding of the sensors (e.g. direct blinding sunlight, highly RADAR-reflective environment);
- (ii) The target vehicle is not extreme with regard to the Radar Cross Section (RCS) or the shape/silhouette (e.g. below fifth percentile of RCS of all M1 vehicles)
- (iii) There are no significant weather conditions affecting the sensing capabilities of the vehicle (e.g. no heavy rain, dense fog, snow, dirt);
- (iv) There are no overhead obstructions close to the vehicle;

**Situation Conditions**

The condition set (again an exhaustive list) that limits the performance of the AEBS probably the most looks at the situation itself. Regardless of the sensor capabilities and the deceleration capabilities, the internal logic of the system needs to be able to make appropriate decisions. Most of the items in this list are there to prevent false-positive braking interventions due to a misunderstanding of the system.

It is expected that increasing experience with systems and the progress of the state of technology might allow to reduce these conditions in the future.

- (d) The situation is unambiguous, i.e.:
  - (i) The preceding vehicle belongs to Category M, N, O3 or O4, is unobstructed, clearly separated from other objects in the driving lane and constantly travelling or stationary;
  - (ii) The vehicle longitudinal centre planes are displaced by not more than 0.2 m;
  - (iii) The direction of travel is straight with no curve, and the vehicle is not turning at an intersection and following its lane.

**Off-Cycle Performance Statement**

The performance requirements paragraph ends with a very important statement, requesting that there shall be no deactivation or switch in the control strategy when the conditions in the condition list are not all met (=one or more of the conditions are not fulfilled).

*When conditions deviate from those listed above, the system shall not deactivate or unreasonably switch the control strategy. This shall be demonstrated in accordance with paragraph 6 and Annex 3 of this Regulation.*

This statement is a key point to achieve robust AEBS performance, yet it is still unclear how this criterion will be verified during type approval or market surveillance processes, especially for the “change of

strategy”, while deactivation can be easily verified. A proposal for some conditions will be made below.

**Numeric Performance Requirements**

Finally, the paragraph closes with a lookup table and interpolation guidance, giving the maximum allowed impact speed as function of the initial relative speed, an excerpt is shown in Table 2. This table defines the required performance for all operating points within the condition set as explained above.

**Table 2: Maximum relative Impact Speed (km/h) (regardless whether target stationary or moving)\***

Relative Speed (km/h)	M3>8t, N2>8t, N3
10	0
20	0
30	0
35	0
40	0
50	0
60	0
70	0
80	28
90	42
100	54***

**Tests**

The test section according to the new approach does no longer define the required performance, as it was the case with implicit requirement definition. On the other hand, the parameter range for expected performance is much larger than for traditional regulations, which makes it virtually impossible to test the system against all parameter combinations.

The test section therefore has two purposes: Its main purpose is to define a minimum set of system tests to ensure a basic safety level in standardized conditions, quite similar to traditional regulations.

Its other purpose is to open up a path for testing different conditions like speeds, surroundings, etc., to verify the full parameter range as specified in the performance requirements, and allow for testing of changing the control strategy.

The core of the test section is paragraph 6.5, which starts with the traditional test description:

**6.5. Warning and Activation Test with a Moving Vehicle Target**

*The subject vehicle and the moving target shall travel in a straight line, in the same*

direction, for at least two seconds prior to the functional part of the test. with a subject vehicle to target centreline offset of not more than 0.2m. Tests shall be conducted with a vehicle travelling at the following relative speeds to the target, with a tolerance of +/- 2 km/h for all tests, and a target travelling at 20 km/h, with a tolerance of +/-2 km/h for both the target and the subject vehicles, but at speeds not beyond the range specified in paragraph 5.2.1.3.:

(a) 20 km/h (e.g. target travelling at 20 km/h, vehicle travelling at 40 km/h, relative speed is 20 km/h);

(b) Maximum required impact avoidance speed as shown in paragraph 5.2.1.4 (e.g. maximum required impact avoidance speed for a N3 vehicle is 70 km/h, target is travelling at 20 km/h, vehicle speed is 90 km/h), and

(c) Either:

(i) Maximum required impact avoidance speed, as shown in paragraph 5.2.1.4., + 8 km/h (e.g. for a target travelling at 20 km/h and a M3 vehicle > 8 tons, the test shall be conducted at 20 + 70 + 8 = 98 km/h), or

(ii) Maximum design speed (e.g. for a target travelling at 20 km/h, speed limiter speed of approximately 89 km/h for an N3),

whichever is lower.

The following paragraph allows to test other conditions. This allows the technical service to perform additional verifications when in doubt, and on the other hand to allow market surveillance authorities to verify every aspect of the performance requirements when re-testing a vehicle.

*If this is deemed justified, the technical service may test in any test condition within the conditions specified in paragraph 5.2.1.4. and with any other speeds listed in the tables in paragraph 5.2.1.4. and within the prescribed speed range as defined in paragraph 5.2.1.3. Outside of the conditions of Paragraph 5.2.1.4., the Technical Service may verify that the control strategy is not unreasonably changed or AEBS switched off. The report of this verification shall be appended to the test report.*

This implementation of the test definitions serves the purpose to have technical services test at least a minimum set of tests, and on the other hand allow technical service and market surveillance to assess the full performance requirements – thus forcing vehicle manufacturers to develop robust systems working under all conditions, especially in real traffic.

## VERIFYING OFF-CYCLE PERFORMANCE FOR AEBS REGULATIONS

While performance requirements over a range of various parameters are clearly defined, and also the deactivation as absence of performance can be identified quite easily, the remaining challenge is how to verify whether a specific system does not unreasonably switch the control strategy when out of these conditions.

### Possible Deceleration Lower Than Reference Case

The aim of this section is to propose criteria for this case, based on the safety models applied during the definition of the recent AEBS regulations.

The required speed reduction has been derived from a simple model with the following parameters:

- the maximum possible deceleration for a given surface, given by the friction coefficient  $\mu$ ,
- the time required to reach the maximum deceleration,  $t_{buildup}$ ,
- the TTC value for the start of brake intervention,  $TTC_{Brake}$ .

With these parameters, the possible avoidance speed would be approximately

$$v_{avoidance} = 2 \cdot \mu \cdot g \cdot (TTC_{Brake} - 0.5 \cdot t_{buildup}),$$

or for situations where the friction is not the issue, but the deceleration is limited to  $d_{lim}$ :

$$v_{avoidance} = 2 \cdot d_{lim} \cdot (TTC_{Brake} - 0.5 \cdot t_{buildup}).$$

For instance, two items from the performance section of Regulation 131-02 look at whether the required deceleration is possible:

(a) Vehicle external influences allow for the required deceleration, i.e.:

(b) The vehicle state itself allows for the required deceleration, e.g.:

An unreasonable switch of the control strategy could in this case be a different, later brake intervention  $TTC_{Brake}$ . The maximum avoidance speed in reference conditions and the expected avoidance speed in lower deceleration conditions should relate to each other according to

$$\frac{v_{avoidance,reference}}{v_{avoidance,lower\ deceleration}} = \frac{\mu \cdot g}{d_{lim}},$$

if the control strategy (=brake intervention timing) is the same.

### Sensor Influences

In conditions under the third item, the target is detected later or not at all, this requires individual experiments to understand whether a control strategy is unreasonably switched or not:

*(c) There are no external influences affecting the physical sensing capabilities, i.e.:*

### Ambiguous Situation

The last remaining item, limiting the required performance to unambiguous situations, is probably the most complex to deal with switching the control strategy:

*(d) The situation is unambiguous, i.e.:*

For its first sub-item, the decelerating target is missing; however, this is simple due to the fact that a numerical speed reduction as function of the relative speed is meaningless when the relative speed changes over time.

One method to identify whether the control strategy is changed could be to compare the TTC for the beginning of the brake intervention with the so-called ‘enhanced TTC’, a variable taking the changing velocities into account [3]:

*(i) The preceding vehicle belongs to Category M, N, O3 or O4, is unobstructed, clearly separated from other objects in the driving lane and constantly travelling or stationary;*

The lateral displacement, or – more important – the overlap between two vehicles determines the last time to steer: the less overlap exists, the more likely is a successful avoidance maneuver quite late before the collision. Identifying whether a control strategy has changed could be done by comparing the TTC for the last time to steer around in reference conditions (+/- 0.2 m as stated below) to the TTC for the last time to steer in the situation under question.

The reference lateral acceleration could be calculated with the assumption

$$\Delta y = a_y t^2,$$

the generic equation for displacement (known from the overlap in the reference case) as function of lateral acceleration  $a_y$  (to be calculated and rechecked for the non-reference situation) and time  $t$ .

*(ii) The vehicle longitudinal centre planes are displaced by not more than 0.2 m;*

For the final sub-item, it is hard to identify a general mathematical method for change of strategy. A proposal could be to identify the horizontal aperture of the sensor system (RADAR and camera) and checking whether the target was within the aperture at all times.

*(iii) The direction of travel is straight with no curve, and the vehicle is not turning at an intersection and following its lane.*

To sum up, there are several methods for identifying whether the control strategy has changed. Whether or not this switch or deactivation is unreasonable will probably require a justification from the vehicle manufacturer.

## IMPLEMENTATION IN REGULATION 151, BLIND SPOT INFORMATION SYSTEMS

### Requirements

Regulation 151 in its original form follows partly the traditional regulation, since it has several pre-defined test cases with implicit specification of the requirements. To still have benefits from the “new approach”, there are several measures in place. The core text of Regulation 151 does give vague requirements and allows the testing of other conditions than those specified in the (implicit) test case table [4]:

*5.3.1.4. The BSIS shall give an information signal at last point of information, for a bicycle moving with a speed between 5 km/h and 20 km/h, at a lateral separation between bicycle and vehicle of between 0.9 and 4.25 metres, which could result in a collision between bicycle and vehicle with an impact position 0 to 6 m with respect to the vehicle front right corner, if typical steering motion would be applied by the vehicle driver.*

*The information signal shall not be visible before the first point of information. It shall be given between the first point of information and the last point of information. The first point of information may be calculated for any impact position by increasing with the difference between 6 m and impact position.*

*It shall also give an information signal if a bicycle is detected at a lateral separation of between 0.25 up to 0.9 m longitudinally at least located at the most forward front wheel while driving straight.*

However, the specifications how this can be achieved are given in the test section, which is not in line with the “new” approach, since this is a further specification of the requirements shown above:

### 6.5. Blind Spot Information Dynamic Test

*6.5.1. Using cones and the bicycle dummy, form a corridor according to Figure 1 in Appendix 1 to this Regulation and the*

additional dimensions as specified in Table 1 of Appendix 1 to this Regulation.

[...]

6.5.10. The test is passed when the Blind Spot Information signal has been activated in all test cases as shown in Table 1 of Appendix 1 to this Regulation before the vehicle has crossed line C (see paragraph 6.5.7. above) and the Blind Spot Information signal has not been activated in any test run when the vehicle passes the traffic sign (see paragraph 6.5.8. above).

For vehicle speeds up to 5 km/h, it is deemed satisfactory if the information signal is activated 1.4 seconds before the bicycle has reached the theoretical collision point as specified in Appendix 1, Figure 1. For vehicle speeds between 5 and 10 km/h, the value  $d_c$  shall be 5 m.

For vehicle speeds above 25 km/h, where the stopping distance is higher than 15 m,  $d_c$  as specified in Appendix 1, Figure 1 shall be as specified in Appendix 1, Table 2.

However, the vague definition of requirements allows an alternative specification for test cases that is more in line with the “new approach”. The so-called “alternative testing annex” has been adopted by WP.29 and will enter into force in May 2023.

- It follows the following principles:
- Generic methods for heavy vehicles turning are given by so-called envelopes through which typical drivers shall navigate the vehicle.
- The trajectory of the vehicle is recorded and then exactly replayed by robot control.
- In the replay, a robot-controlled bicycle dummy is added so that a collision will occur.
- Finally, the information signal timing is checked for sufficient stopping time (i.e. was it possible with a deceleration of  $5 \text{ m/s}^2$  and a reaction time of 1.4 seconds after the blind stop information signal was given to avoid the accident?).

This new approach here forces manufacturers to specify their system for traffic safety and makes a fine-tuning towards few test cases impossible.

## TEST EQUIPMENT

The new approach requires equipment beyond what is currently used in type-approval testing:

- a precise position measurement system for the vehicle in order to identify whether the vehicle was within the operating range,
- driving robots to make the ego vehicle as well as the target systems follow precisely programmed trajectories,

- several exactly controllable target systems that allow to approach the borders of the operating range as close as possible.

### Position measurement systems

State of the art in position measurement nowadays are sensor fusion systems with differential GNSS and inertial measurement units. These devices achieve an accuracy up to  $\pm 1 \text{ cm}$ , with typical values below  $\pm 10 \text{ cm}$ . An example for such a system, fitted to a test vehicle, is shown in Figure 2 below.

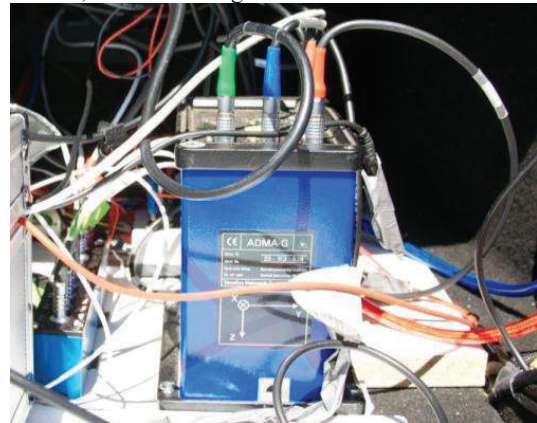


Figure 2: DGPS and inertial measurement system

### Driving Robot Systems

Based on precise position measurement, driving robots control any given vehicle by modulating their driving controls (steering wheel, accelerator and brake pedals). The achieved accuracy varies with dynamics, vehicle and how well the robot systems are tuned towards the concrete vehicle and lie in the order of magnitude of 10-50 cm even in complex turning situations. See Figure 3 below for an example of a vehicle.





**Figure 3: Steering and pedal actuators, mounted in a N<sub>3</sub> tractor vehicle**

### Robotic Target Systems and Targets

Robotic target carriers are flat over-runnable platforms where a variety of surrogate targets resembling passenger cars, pedestrians, bicycles or motorcycles can be fitted, see Figure 4 to Figure 7. The platforms include a precise position measurement system and control logics comparable to the driving robot systems, allowing them to achieve approximately the same precision in control.

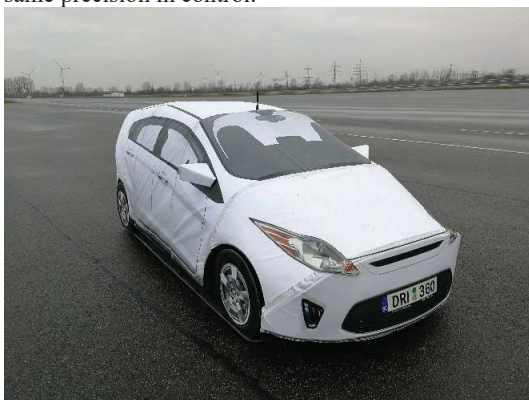


**Figure 4: Car dummy on robotic target carrier**



**Figure 5: Bicycle dummy on robotic target carrier**

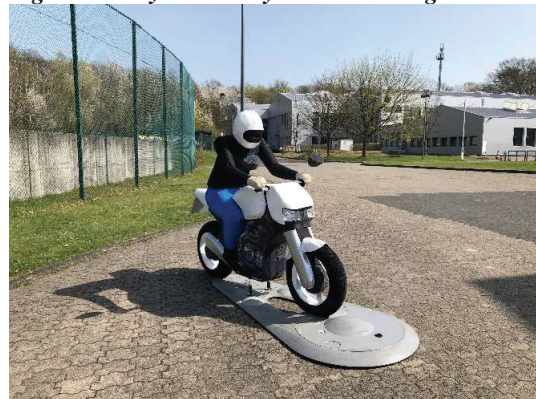


**Figure 6: Motorcycle dummy on robotic target carrier**



**Figure 7: Pedestrian dummy on robotic target carrier**

### CONCLUSIONS

A new approach for the formulation of vehicle technical regulations has been presented that is specifically helpful for advanced driver assistance system and automated driving system regulations, but for some others as well.

The aim of this new approach is to make design of systems simply towards test criteria impossible and to force manufacturers to develop robust systems that will deliver the required performance in realistic surroundings.

This is achieved by three measures: First, by precise formulation of verifiable performance requirements over the whole relevant operating range, and asking for no unreasonable change of the system strategy outside of this operating range. Second, by allowing tests in all operating points to be performed, so that it is unclear in the beginning as to what exactly could be tested, besides a set of standard tests (that still are defined in the regulations and will always be tested). Third, not part of the regulation itself, by a market surveillance system that allows retest of randomly selected or suspicious vehicles by independent authorities against the regulations.

The implementation of these three measures in new regulations as well as appropriate measurement equipment has been shown in the paper.

The new approach however brings also a shift of responsibility for defining test cases from the regulator towards the technical services and towards the market surveillance authorities, requires more test cases to be

conducted and more considerations on what is a relevant and valuable test to assess the vehicle or system characteristics.

## REFERENCES

- [1] United Nations Economic Commission for Europe: Regulation (UN) No. 131-02. Available as document GRVA-14-50-rev1 for download at <https://unece.org/sites/default/files/2022-01/GRVA-12-50r1e.pdf>.
- [2] United Nations Economic Commission for Europe: Regulation (UN) No. 157. Available for download at <https://unece.org/sites/default/files/2021-03/R157e.pdf>.
- [3] Winner, Hermann: “Grundlagen von Frontkollisionsschutzsystemen“. In: Winner et al (Editors): “Handbuch Fahrerassistenzsysteme“. P. 893-912. 3. Edition, Springer Verlag, Wiesbaden, 2015.
- [4] United Nations Economic Commission for Europe: Regulation (UN) No. 151. Available for download at <https://unece.org/sites/default/files/2021-08/R151e.pdf>.